














Muscle-specific Cand2 is translationally upregulated by mTORC1 and promotes adverse cardiac remodeling

Agnieszka A Górski^{1,2,†} , Clara Sandmann^{1,2,†} , Eva Riechert^{1,2} , Christoph Hofmann^{1,2} , Ellen Malovrh^{1,2} , Eshita Varma^{1,2} , Vivien Kmietyk^{1,2} , Julie Ölschläger^{1,2}, Lonny Jürgensen^{1,2}, Verena Kamuf-Schenk^{1,2}, Claudia Stroh^{1,2}, Jennifer Furkel^{1,2} , Mathias H Konstandin^{1,2}, Carsten Sticht³, Etienne Boileau^{1,2,4} , Christoph Dieterich^{1,2,4} , Norbert Frey^{1,2}, Hugo A Katus^{1,2}, Shirin Doroudgar^{1,2} & Mirko Völkers^{1,2,*} 

Abstract

The mechanistic target of rapamycin (mTOR) promotes pathological remodeling in the heart by activating ribosomal biogenesis and mRNA translation. Inhibition of mTOR in cardiomyocytes is protective; however, a detailed role of mTOR in translational regulation of specific mRNA networks in the diseased heart is unknown. We performed cardiomyocyte genome-wide sequencing to define mTOR-dependent gene expression control at the level of mRNA translation. We identify the muscle-specific protein Cullin-associated NECD8-dissociated protein 2 (Cand2) as a translationally upregulated gene, dependent on the activity of mTOR. Deletion of Cand2 protects the myocardium against pathological remodeling. Mechanistically, we show that Cand2 links mTOR signaling to pathological cell growth by increasing Grk5 protein expression. Our data suggest that cell-type-specific targeting of mTOR might have therapeutic value against pathological cardiac remodeling.

Keywords Cand2; cardiac; hypertrophy; mTOR

Subject Category Molecular Biology of Disease

DOI 10.15252/embr.202052170 | Received 29 November 2020 | Revised 26

August 2021 | Accepted 10 September 2021 | Published online 4 October 2021

EMBO Reports (2021) 22: e52170

Introduction

Pathological cellular remodeling is a hallmark of heart failure (HF) independent from the underlying etiology such as pressure overload, myocardial infarction, or inherited cardiomyopathies. Several

studies and our recent work revealed that pathological cardiac stress induces early morphological changes and cardiac hypertrophy due to the activation of the kinase mechanistic target of rapamycin complex 1 (mTORC1; Buss *et al*, 2009; Zhang *et al*, 2010; Völkers *et al*, 2013; Sciarretta *et al*, 2018). mTORC1 promotes protein synthesis by induction of rRNA transcription, ribosomal protein synthesis, and phosphorylation of translation initiation factors and enhances translation of specific mRNAs for stress adaptation (Ma & Blenis, 2009; Iadevaia *et al*, 2012). Mechanistically, mTORC1 promotes translation of a specific subset of mRNAs regulated by the translation initiation factor eIF4E by direct phosphorylation of the eIF4E binding proteins (4E-BPs; Hsieh *et al*, 2012; Thoreen *et al*, 2012). mTORC1-sensitive transcripts often contain a terminal oligopyrimidine (TOP) or TOP-like motif in the 5' UTR (5' untranslated region) and are predominantly regulated on the translational level (Jefferies *et al*, 1994; Avni *et al*, 1996; Thoreen *et al*, 2012).

Systemic pharmacological or genetic mTORC1 inhibition prevents pathological hypertrophy and improves cardiac function in murine disease models (Shioi *et al*, 2003; Buss *et al*, 2009; Völkers *et al*, 2013), but no established therapeutic regime targets mTORC1 at the level of cardiomyocytes in patients yet. Moreover, the role of mTORC1 in translational regulation of specific mRNA networks in the diseased heart is mainly unknown, partly because existing tools in previous studies were unable to analyze gene expression at the level of translation.

We aimed to characterize mTORC1-dependent changes in gene expression that mediate cardiac response to pathological stress. Ribosome profiling (Ribo-seq) was used to obtain quantitative measurements of translation and to dissect the mTORC1-dependent translational regulation of gene expression in cardiomyocytes.

1 Department of Cardiology, Angiology and Pneumology, University Hospital Heidelberg, Heidelberg, Germany

2 DZHK (German Centre for Cardiovascular Research), partner site, Heidelberg/Mannheim, Germany

3 Medical Research Center, Medical Faculty Mannheim, Heidelberg University, Mannheim, Germany

4 Section of Bioinformatics and Systems Cardiology, Department of Cardiology, Angiology, and Pneumology and Klaus Tschira Institute for Integrative Computational Cardiology, University of Heidelberg, Heidelberg, Germany

*Corresponding author. Tel: +49 6221 56 8676; E-mail: mirko.volkers@med.uni-heidelberg.de

†These authors contributed equally to this work

Among other genes dependent on the activity of mTORC1, we identified the muscle-specific gene cullin-associated NEDD8-dissociated protein 2 (Cand2). Initially named transcription factor TATA-binding protein 120B (TIP120B), Cand2 belongs to the TIP120 gene family and shares 60% homology with TIP120A (Cand1) (Aoki *et al*, 1999).

In contrast to ubiquitously expressed Cand1, Cand2 is a muscle-specific protein and has been identified only in mammals. Both proteins have been shown to directly bind and modulate the activity state of Cullin1 (Cul1) (Liu *et al*, 2002; Goldenberg *et al*, 2004; Shiraiishi *et al*, 2007). Cul1 is a component of SCF-like E3 ligase complex that promotes ubiquitination (Furukawa *et al*, 2000; Zheng *et al*, 2002; Zou *et al*, 2018). The activation of the SCF complex is stimulated by reversible and covalent posttranslational modification, neddylation of Cul1, which relies on ligation of the ubiquitin-like protein NEDD8 to a specific lysine residue in the C terminus (Goldenberg *et al*, 2004; Min *et al*, 2005).

We found that pressure overload induced Cand2 expression at the level of translation which was dependent on the activity of mTORC1. Functionally, Cand2 was required and sufficient for pathological remodeling, and Cand2 knockout (KO) mice were protected against pathological remodeling. Mechanistically, we found that Cand2 controls the expression of G protein-coupled receptor 5 (Grk5) expression *in vitro* and *in vivo*, which in turn is linked to transcription of hypertrophic genes driven by myocyte enhancer factor 2 (MEF2).

Our data highlight a mechanism, where translational, mTORC1-dependent, control of Cand2 expression results in increased expression of Grk5, which leads to transcriptional reprogramming in diseased cardiomyocytes (mRNA translation controls transcriptional activity). This links mTOR-dependent cytosolic signaling events that drive specific mRNA translation to transcriptional activity.

Results

Cand2 is a myocyte-specific protein translationally upregulated during pathological stress

To define mRNAs translationally regulated by mTOR signaling in response to pathological cell growth, cultures of neonatal rat ventricular cardiomyocytes (NRCMs) were acutely treated for 3h with the α -1 adrenoreceptor agonist phenylephrine (50 μ M, PE) and with Torin 1 (100 nM), which inhibits mTOR by binding to the ATP-binding site in the kinase domain (Thoreen *et al*, 2012). Specific inhibition of mTOR-dependent protein signaling by Torin 1 was confirmed by immunoblots (Fig EV1A), while other signaling pathways such as Erk1/2 and p38 signaling were unaffected by Torin 1. Ribosome profiling (Ribo-seq, ribosomal sequencing) has emerged as a quantitative technique to study global gene expression. It overcomes some limitations of classical expression analysis, as it directly quantifies the number of translating ribosomes (Ingolia *et al*, 2009). The effect of Torin 1 on mRNA translation was analyzed by Ribo-seq in cultured cardiomyocytes (Fig 1A). Total cellular RNA was collected for parallel RNA-seq (RNA sequencing) to quantify mRNA abundance (full list is provided in Dataset EV1).

We identified 199 genes that were decreased and 165 that were increased (\log_2 FC < -1 or > 1) in Ribo-seq in an mTOR-dependent

manner in response to PE treatment (Fig 1B). Among the suppressed genes, 17% have a known TOP or TOP-like motif in the 5' UTR (Fig 1C), which is known to be sensitive to mTOR inhibition (Thoreen *et al*, 2012), and the suppressed genes are predominantly regulated on the translational level (Fig 1D). Immunoblotting confirmed a decrease in the expression of selected mTOR-dependent genes such as eEF2 and RpS5 at the protein level upon Torin 1 treatment (Fig EV1B), but not at the transcript level. Molecular markers of pathological growth such as *Nppb* or *Xirp2* were blocked while *Nppa* was still induced (Fig EV1C). Stimulation of NRCMs with PE resulted in a strong increase in mRNAs in polysomal fractions (Fig EV1D). The increase of mRNAs in the polysomal fraction induced by PE was blocked by Torin 1, confirming that Torin 1 blocks the recruitment of ribosomes into polysomal fractions. The effects of mTOR inhibition on cardiomyocyte growth were examined in isolated cardiac myocytes stimulated with PE for 24 h. Torin 1 inhibited PE-induced hypertrophy as assessed by cell surface area measurements (Fig EV2A). To measure the effect of Torin 1 on cap-dependent translation in cells, we used a dual-luciferase reporter vector that distinguishes cap-dependent versus cap-independent translation by separating *Renilla* luciferase from firefly with the poliovirus IRES (Poulin *et al*, 1998; Fig EV2B). Therefore, the *Renilla*/firefly ratio would determine translation initiation mechanism. Torin 1 inhibited cap-dependent but not IRES-dependent translation measured by luciferase activity.

In line with the *in vitro* data, mTOR inhibition with Torin 1, *in vivo*, blocked pathologic growth as well as induction of *Nppa* and *Nppb* induced by acute transverse constriction (TAC) surgery, a common model for cardiac hypertrophy and remodeling (Fig EV2C and D; Doroudgar *et al*, 2019). Thus, mTOR-dependent and cap-dependent protein synthesis are increased during hypertrophic growth and this is necessary for induction of cell growth, *in vitro* and *in vivo*.

Gene ontology (biological processes) analysis of the genes that were suppressed by Torin 1 showed strong enrichment for those involved in translation, metabolism, as well as signaling cascades (Fig 1E). Overall, this dataset defined a specific subset of genes that are regulated in a mTOR-dependent manner in response to neurohumoral stimulation with PE. Next, we followed our identified mTOR-dependent genes in a previously published *in vivo* data set after TAC surgery (Doroudgar *et al*, 2019). mTOR-dependent genes were translationally upregulated in response to TAC surgery (Fig 1F and G). Increased expression of identified mTOR targets independent from changes of transcript levels such as eEF2, desmin, rpS5, or rpS20 was confirmed using immunoblots and RT-qPCRs from heart lysates after TAC surgery (Fig 1H and I). Consistent with these results, protein levels of eEF2, desmin, rpS20 as well as 4ebp1 increased after TAC, but Torin 1 blocked the induction (Fig 1J). Consistent with the Ribo-Seq data *in vitro*, mRNA levels quantified by RT-qPCR were unaffected by TAC surgery and Torin 1 treatment (Fig 1K).

Among the 199 genes with decreased translation upon Torin 1 treatment *in vitro*, 17 were significantly increased in the *in vivo* data set after TAC surgery (Doroudgar *et al*, 2019; Fig 2A). Among this subset of genes that were increased by pressure overload *in vivo* and dependent on mTOR activity *in vitro* was the muscle-specific protein Cand2¹² (Fig 2A). Since its function in cardiomyocytes was completely unknown, we aimed to characterize the role of Cand2 during pathological remodeling. Torin 1-induced downregulation of

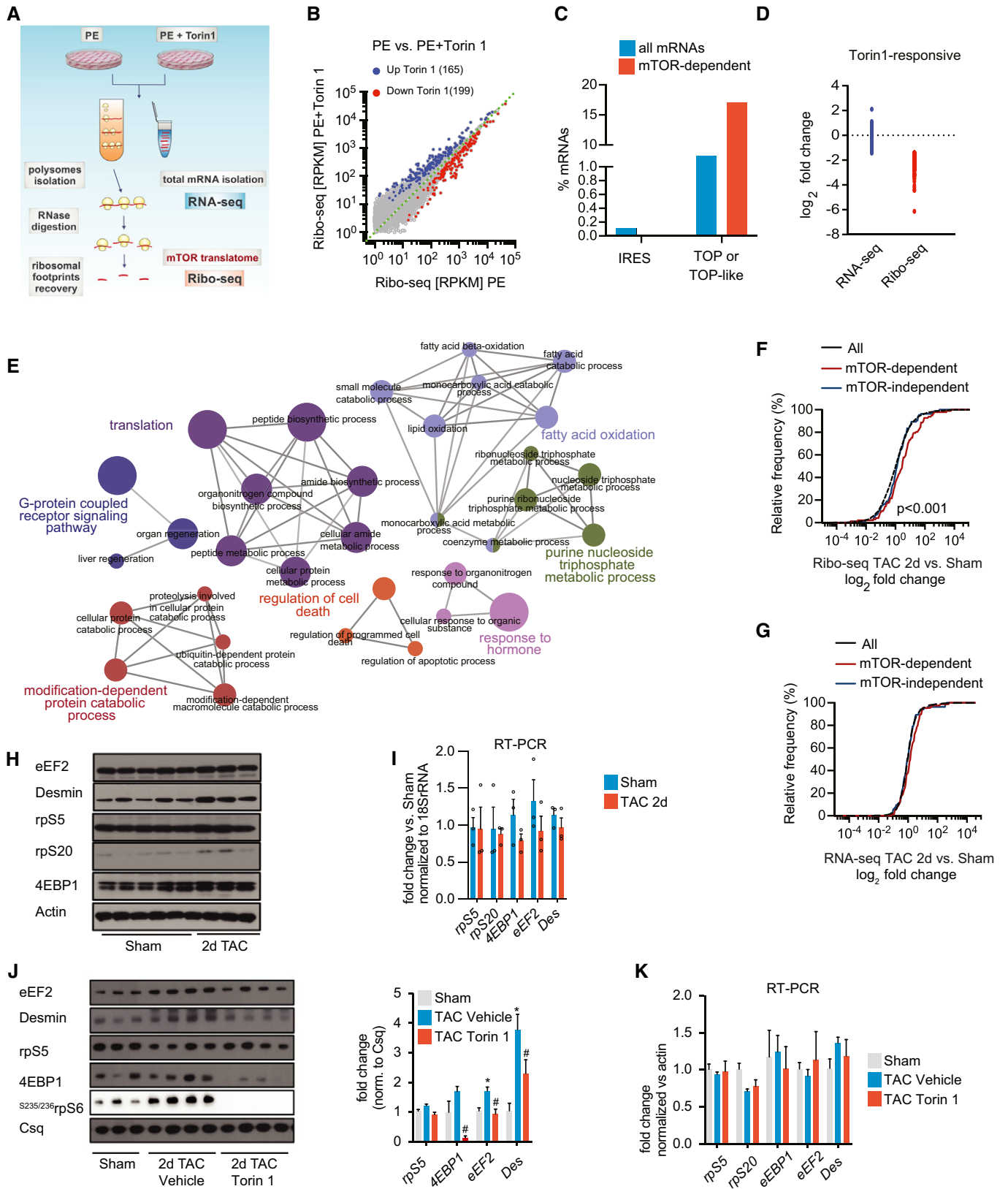


Figure 1.

Figure 1. Identification of the mTORC1-dependent cardiac translome.

- A Experimental design of translational profiling of mTOR-dependent mRNAs *in vitro* in NRCMs. Polysomal fractions were isolated on sucrose gradient and ribosomal footprints were recovered by ribonuclease digestion. NRCMs were treated with vehicle or Torin 1 (100 nM for 3 h) to block the mTOR pathway.
- B Scatter plot of ribosome occupancy in Ribo-seq of cultured cardiomyocytes in response to PE and Torin 1 treatment (blue dots—mRNAs upregulated after Torin 1, red dots—downregulated mRNA. RPKM—Reads per kilobase million).
- C Percentage of IRES (Internal Ribosomal Entry Site) and TOP or TOP-like containing mRNAs in total and Torin 1-sensitive mRNA pools.
- D Transcriptional (RNA-seq) vs. translational (Ribo-seq) control of mTOR-regulated mRNAs.
- E Network of enriched GO categories (biological process) among mTOR-sensitive genes into several functional groups represented by circles of different colors. Each node represents one enriched GO category with the size of the node is proportional to the number of transcripts. Edges indicate similarity (between the two connected GO categories).
- F, G Cumulative fraction of mRNAs relative to their fold change of Ribo-seq and RNA-seq between all and mTOR-dependent transcripts two days after TAC surgery. Kolmogorov–Smirnov–Wallis test.
- H, I Immunoblot and RT-qPCR representing levels mTOR-dependent targets with defined 5'TOP motifs 3 h and 2 days after TAC. $n = 3$ biological replicates per condition.
- J Immunoblots and quantifications of protein expression of mTOR targets two days after TAC surgery and after mTOR inhibition with Torin 1. $*P \leq 0.05$ vs. sham surgery, $\#P \leq 0.05$ vs. TAC 2d surgery. t -test, $n = 5$ biological replicates per group.
- K RT-qPCR for indicated mRNAs 2 days after TAC for indicated groups, $n = 5$ biological replicates per group.

Data information: Error bars indicate means \pm SEM.

Source data are available online for this figure.

Cand2 translation was not due to transcriptional regulation assessed by parallel RNA-seq (Fig 2B). mTOR activity increased Cand2 protein levels *in vitro*, as well, but had no impact on its transcript levels measured by RT-qPCR (Fig 2C and D), confirming the results from the Ribo-seq data sets. Ribo-seq data revealed an increased expression of Cand2 two days after TAC (Fig 2E). Torin 1 inhibited Cand2 expression also without pharmacological stimulation of NRCMs (Fig EV2F). In contrast, protein expression of Cand1 did not change after TAC surgery *in vivo* or after PE treatment of NRCMs *in vitro* (Fig EV2F).

In vivo, Cand2 translation was unchanged in early (3 h after TAC) pressure overload (Fig 2F and G). Translational upregulation of Cand2 in the heart was detected on the protein level when compared by immunoblotting to sham-operated mice (Fig 2H). Increased Cand2 levels *in vivo* were not caused by increased Cand2 transcript levels as shown by RT-qPCR (Fig 2I). To assess whether mTORC1 controls Cand2 expression *in vivo*, Torin 1 was injected in mice after TAC or sham surgery and Cand2 levels were assessed by immunoblotting (Fig 2H). Along with rpS6 phosphorylation inhibition by Torin 1, increased Cand2 protein levels after TAC surgery were completely blocked by Torin 1, suggesting that Cand2 mRNA belongs to mTORC1-sensitive genes, *in vivo*, as well. Since mTORC1 specifically regulates translation of mRNAs with 5'TOP motifs, we placed the 5' UTR of Cand2 mRNA upstream of *Renilla* luciferase to investigate its regulatory potential in a mTORC1-dependent manner (Fig 2J). Cand2 5' UTR showed a similar degree of reporter inhibition after Torin 1 treatment as the known TOP motif-containing 5' UTR of eEF2. This confirmed mTORC1-dependent translation of Cand2 and suggests the presence of a regulatory motif in its 5' UTR. Taken together, mTORC1 controls the expression levels of Cand2 in response to pathological stimulation both *in vitro* and *in vivo*.

To further characterize Cand2, we analyzed its expression profile in different organs in mice. Consistent with a previous report (Aoki *et al*, 1999), Cand2 protein was expressed predominantly in muscle tissues (Fig 3A). qRT-PCR analysis also revealed the highest Cand2 mRNA level in the heart (Fig 3B). Immunofluorescent staining confirmed specific Cand2 expression only in cardiomyocytes (Fig 3C). In addition, immunoblots from isolated cardiac cells showed Cand2

expression only in cardiomyocytes but not in endothelial cells or fibroblasts (Fig 3D), suggesting that Cand2 protein expression is restricted to muscle cells in the heart. Subsequently, we analyzed Cand2 subcellular localization in isolated cardiomyocytes by immunofluorescent staining (Fig 3E). Consistent with studies on skeletal muscle cell maturation (Shiraishi *et al*, 2007), endogenous Cand2 was located in the nucleus and cytoplasm in cardiomyocytes. Subcellular fractionation of the left ventricle (LV) confirmed the cytoplasmic and nuclear distribution of Cand2 (Fig 3F).

Cand2 contributes to cardiomyocytes pathological growth *in vitro* and *in vivo*

Next, we studied the effect of Cand2 on cardiomyocyte cell size after Cand2 knockdown (KD) or overexpression (OE) (Fig 4A and B). Cand2 depletion *in vitro* decreased cell surface area and blunted the response to neurohormonal stimulation with PE treatment (Fig 4C and D). In contrast, Cand2 overexpression induced cardiomyocyte growth, and the increase in cell size after overexpression was comparable to control PE-treated cells (Fig 4E). *Nppa* levels correlated to Cand2 expression: decreased when Cand2 was depleted and elevated in Cand2 overexpression in untreated and PE stimulated cardiomyocytes (Fig 4F).

To study the role of Cand2 *in vivo*, a novel Cand2 knockout (KO) mouse was generated (Fig EV3A). Cand2-deficient mice were viable and cardiac function as assessed by ejection fraction, as well as left ventricle weight to body weight (LV/BW) ratio remained unchanged compared to littermate control animals (Fig EV3B and C). In line with this, Cand2 KO did not alter the levels of fetal gene markers normally upregulated in the adult heart during stress, such as *Nppa* and *Nppb* (Fig EV3E and F). Moreover, Cand2 knockout did not disturb the levels of Cand1 (Fig EV3D).

Next, Cand2 KO mice along with wild-type (WT) littermates were subjected to TAC or sham surgery and phenotypic consequences were analyzed two weeks after surgery. TAC surgery resulted in decreased ejection fraction, fractional shortening, and increased LV/BW ratio in WT mice (Fig 4G and I). In contrast, Cand2-deficient mice showed preserved cardiac function as well as significantly decreased LV/BW ratio compared to TAC-operated WT mice.

Moreover, TAC-induced *Nppa* and *Nppb* levels in WT mice were 1.9-fold and threefold reduced in *Cand2* KO mice, respectively (Fig 4J). Serial echocardiographic analysis revealed improved function of *Cand2* KO mice four weeks after surgery compared to WT mice (Fig EV3G). Overall, these results suggest that *Cand2* deletion protects against pathological remodeling in response to pressure overload.

Cand2 controls Grk5 expression and affects MEF2-dependent transcription

Next, we performed transcriptome profiling of left ventricles from wild-type and *Cand2* KO mice to identify targets that *Cand2* might

regulate (full list in Dataset EV2). mRNA sequencing identified only small changes in the transcriptome when *Cand2* was deleted (Fig 5A). Interestingly, pathway analysis revealed that most *Cand2*-dependent genes are enriched for categories regulating transcription and proteasomal function. Among the *Cand2*-dependent group of genes involved in transcriptional control, the G protein-coupled receptor kinase 5 (*Grk5*) was one of the strongest regulated genes in *Cand2* knockout mice (Fig 5A). While the canonical role of *Grk5* is to phosphorylate agonist bound G protein-coupled receptors, which promotes the binding of arrestin to the receptor, resulting in subsequent desensitization of the receptor, *Grk5* has been found to localize to the nucleus *via* a nuclear localization (NLS) sequence. Previous work showed that following pressure overload, *Grk5*

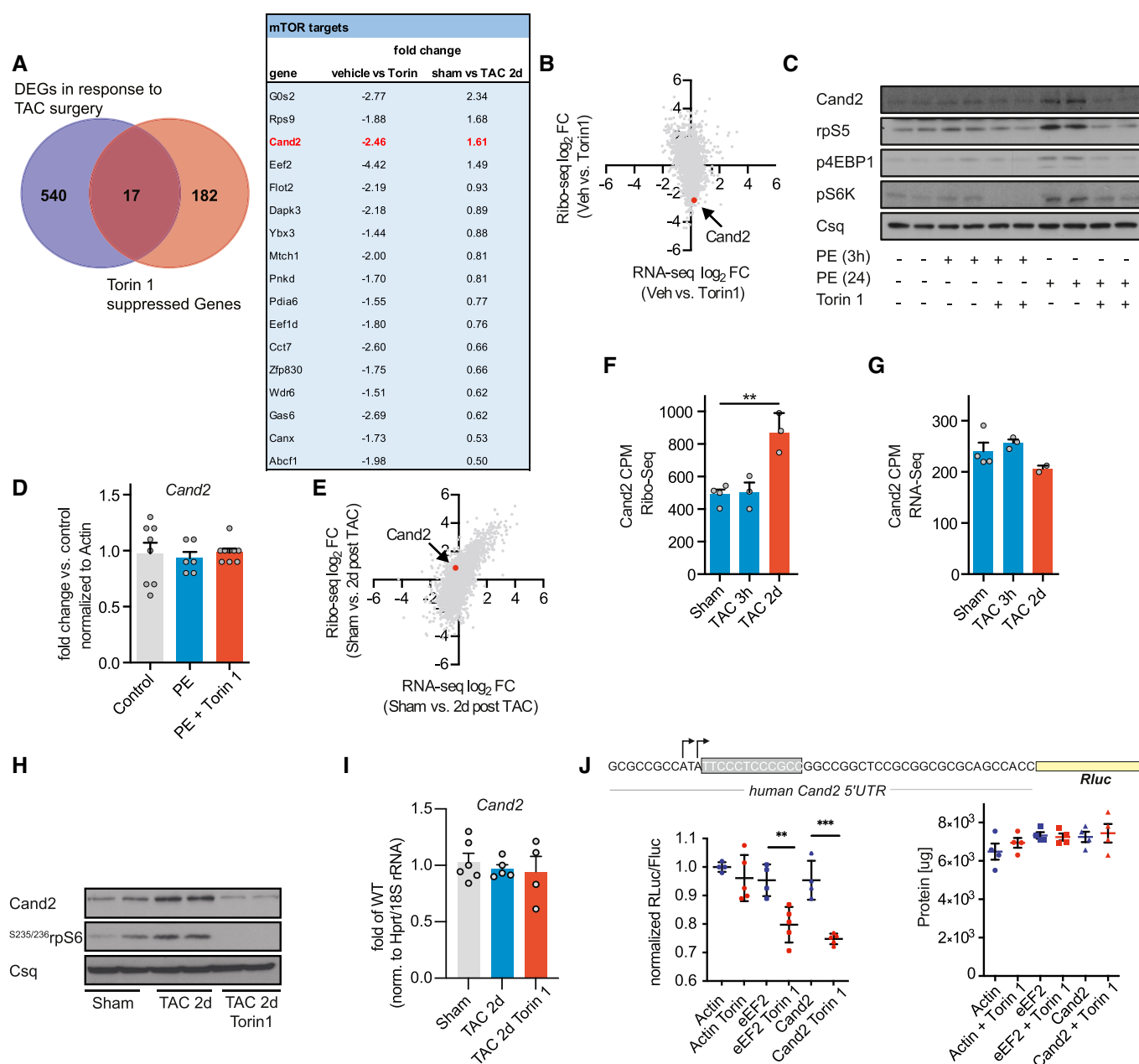


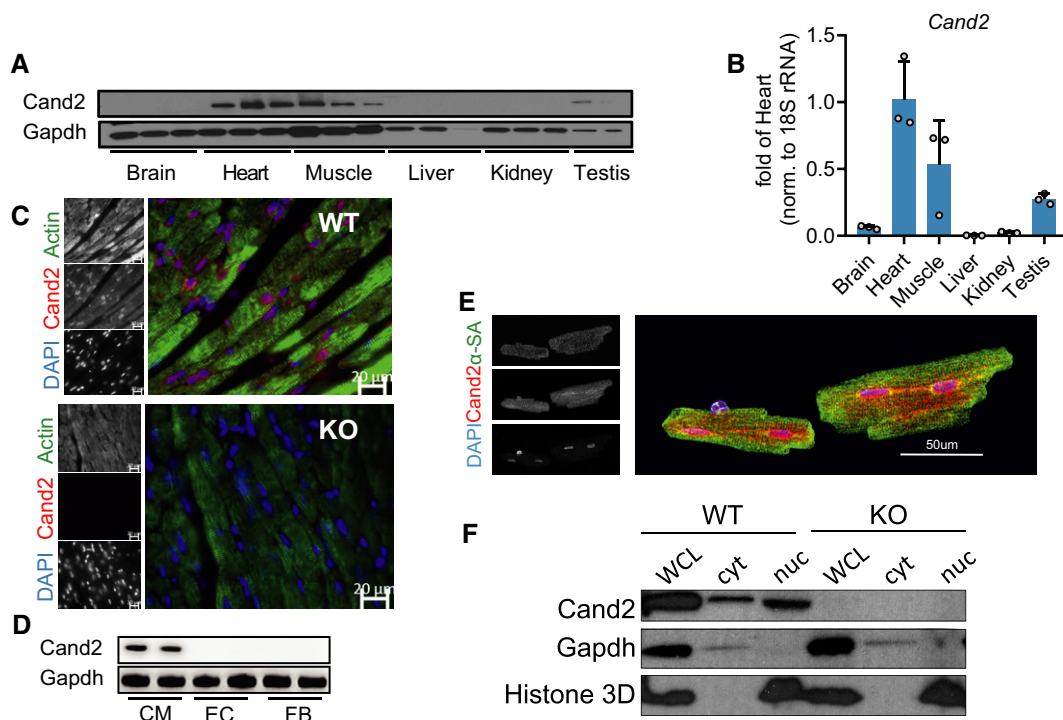
Figure 2.

Figure 2. Cand2 is translationally upregulated during cardiac pathological stress.

- A Venn diagram showing a group of transcripts translationally upregulated *in vivo* 2 days after TAC (DEGs—differentially expressed genes) and regulated by mTORC1 *in vitro* in NRCMs treated with Torin 1. Table with top translationally regulated mTOR-dependent transcripts *in vitro* after Torin 1 treatment of NRCMs and *in vivo* after TAC. Cand2 highlighted in red.
- B Scatter plot of Ribo-seq vs. RNA-seq upon NRCMs treatment of Torin 1 shows Cand2 among translationally downregulated mRNAs. FC—fold change, Veh—vehicle.
- C Protein expression of Cand2 in NRCMs treated with PE for 3 and 24 h, and 24 h of Torin 1 treatment. mTORC1 induction was monitored by downstream targets, p4EBP1, pS6K and rpS5 proteins. Csq—calsequestrin used as a housekeeping protein.
- D Cand2 mRNA levels in NRCMs treated with PE and Torin 1 measured by RT-qPCR. $n = 6-9$ of biological replicates per conditions.
- E Scatter plot of Ribo-seq vs. RNA-seq 2 days after TAC showing an increase of Cand2 translation.
- F, G Ribo-seq and RNA-seq expression data of Cand2 in sham and TAC-operated animals (CPM—count per million). One-way ANOVA, $**P \leq 0.01$, $n = 2-4$ biological replicates per group.
- H Immunoblots of Cand2 expression in left ventricles 2 days post-TAC and after injection with Torin 1. ^{5235/236}rpS6 was used to control the mTORC1 activation. Csq—calsequestrin used as a housekeeping protein.
- I Cand2 mRNA levels 2 days after TAC and after Torin1 injection measured by RT-qPCR. $n = 4-6$ biological replicates per mice group.
- J Schematic representation of reporter consisting of human Cand2 5'UTR and downstream *Renilla* luciferase coding sequence. A potential TOP-like motif is highlighted in a gray box. Black arrows indicate transcription start sites in the adult heart according to the Database of Transcriptional Start Sites (Release 10.1). The effect of Cand2 5'UTR on translation measured by luciferase activity in normal conditions and after mTORC1 block with Torin 1. eEF2—positive control of reporter with defined 5'TOP motif and non-TOP 5'UTR of β -actin used as a negative control. Total protein content in lysates used for luciferase assay. *t*-test, $n = 4-5$ biological replicates per group, $**P \leq 0.01$, $***P \leq 0.001$.

Data information: Error bars indicate means \pm SEM.

Source data are available online for this figure.

**Figure 3. Cand2 is a muscle-specific protein.**

- A Representative immunoblot of Cand2 protein levels in mouse organs.
- B Cand2 expression in mouse organs measured by RT-qPCR. $n = 3$ biological replicates.
- C Immunofluorescent staining of paraffin sections from hearts from WT and Cand2 KO mice. Cand2 (stained in red), Actin (stained in green), and nuclei (stained with DAPI, blue). Scale bar 20 μ m.
- D Representative immunoblot of Cand2 protein from different cardiac cell types CM—cardiomyocytes, EC—endothelial cells, FB—fibroblast.
- E Immunofluorescence of adult rat cardiomyocytes of Cand2 (stained in red), sarcomeric actin (stained in green), and nuclei (stained with DAPI blue). Scale bar 50 μ m.
- F Immunoblot of subcellular fractionation of left ventricle (LV). Gapdh and histone 3D (H3D) used as cytoplasmic and nuclear markers, respectively. WCL—whole-cell lysate, cyt—cytoplasmic fraction, nuc—nuclear fraction.

Source data are available online for this figure.

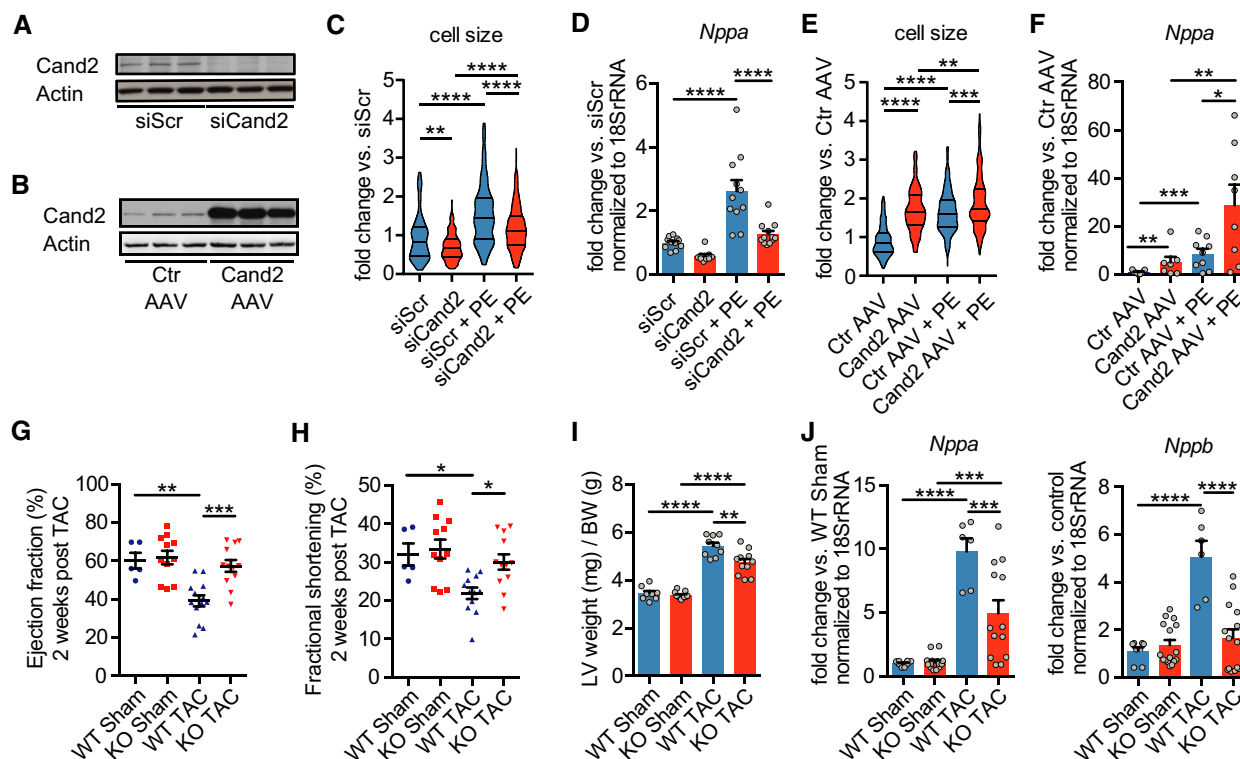


Figure 4. Cand2 is required for cardiac hypertrophy induction.

A Representative immunoblot of Cand2 KD in NRCMs with Cand2-targeting siRNA (siScr—control scrambled siRNA).

B Cand2 OE in NRCMs (Cand2 AAV6; Ctr AAV—control AAV6 vector) analyzed by Western blot.

C Cell surface area measurement of NRCM after Cand2 KD and 24 h PE stimulation. Analyzed by one-way ANOVA. $n > 150$ cells from $n = 3$ independent experiments. Violin plot: the middle horizontal lane—median, upper lane—3rd quartile, lower lane—1st quartile.

D RT-qPCR analysis of *Nppa* transcript level after Cand2 KD and PE treatment of NRCMs. Analyzed by one-way ANOVA. $n = 11$ –12 biological replicates per conditions.

E NRCMs size measurement after Cand2 OE and 24 h PE stimulation. Analyzed by one-way ANOVA. $n > 150$ cells from $n = 3$ independent experiments. Violin plot: the middle horizontal lane—median, upper lane—3rd quartile, lower lane—1st quartile.

F *Nppa* mRNA levels *in vitro* after Cand2 OE and PE treatment measured by RT-qPCR. Analyzed by one-way ANOVA. $n = 5$ –9 biological replicates per conditions.

G Ejection fraction 2 weeks after TAC in WT and Cand2 KO mice measured by echocardiography. Analyzed by one-way ANOVA. $n = 5$ –13 biological replicates per group.

H Fractional shortening 2 weeks after TAC in WT and Cand2 KO mice measured by echocardiography. Analyzed by one-way ANOVA. $n = 5$ –13 biological replicates per mice group.

I LV weight to body weight ratio of WT and Cand2 KO mice subjected to sham and TAC surgeries. Analyzed by one-way ANOVA. $n = 7$ –11 biological replicates per condition.

J *Nppa* and *Nppb* mRNA levels 4 weeks after TAC in WT and Cand2 KO mice measured by RT-qPCR. Analyzed by one-way ANOVA. $n = 6$ –13 mice per group.

Data information: Error bars indicate means \pm SEM; * $P \leq 0.05$, ** $P \leq 0.01$, *** $P \leq 0.001$, **** $P \leq 0.0001$. Source data are available online for this figure.

accumulates in the nucleus of cardiomyocytes and acts as a class II histone deacetylase (HDAC) kinase, phosphorylating HDAC5 specifically, leading to its nuclear export and de-repression of the transcription factor MEF2 (Zhang *et al.*, 2011).

We first analyzed Grk5 expression after gain or loss of function of Cand2 *in vitro* in NRCMs (Fig 5B and C). Cand2 overexpression increased Grk5 protein in NRCMs but did not change its mRNA levels. In contrast, Grk5 protein was downregulated in Cand2 knockdown and Grk5 transcript level remained unaffected. We further analyzed levels of Grk5 in Cand2 KO mice in TAC-induced pressure overload 2 weeks after surgery (Fig 5D). Quantitative RT-PCR analysis did not reveal any significant changes in Grk5 mRNA levels after TAC in Cand2 KO mice compared to WT (Fig 5E). In line with other reports, Grk5 protein was highly increased in TAC-

operated WT mice compared to sham-operated mice. Lack of Cand2 led to an approximately twofold decrease of Grk5 protein levels after TAC. Since Grk5 has been shown to translocate to the nucleus of cardiomyocytes following pressure overload *via* its NLS (Johnson *et al.*, 2004; Martini *et al.*, 2008; Gold *et al.*, 2013), we examined Grk5 levels in the cytoplasm and nucleus *in vivo* in Cand2 KO mice (Fig 5F). Neither TAC nor lack of Cand2 affected Grk5 levels in the cytoplasmic fraction, but Grk5 levels significantly increased in the nucleus in WT mice in response to TAC, which was blocked in Cand2 KO mice.

Since Grk5 regulates the activity of the transcription factor MEF2, we analyzed MEF2 activity by using a luciferase reporter assay. Cand2 knockdown decreased MEF2 luciferase activity by 3.5-fold *in vitro* (Fig 6A). Moreover, the expression of MEF2-dependent

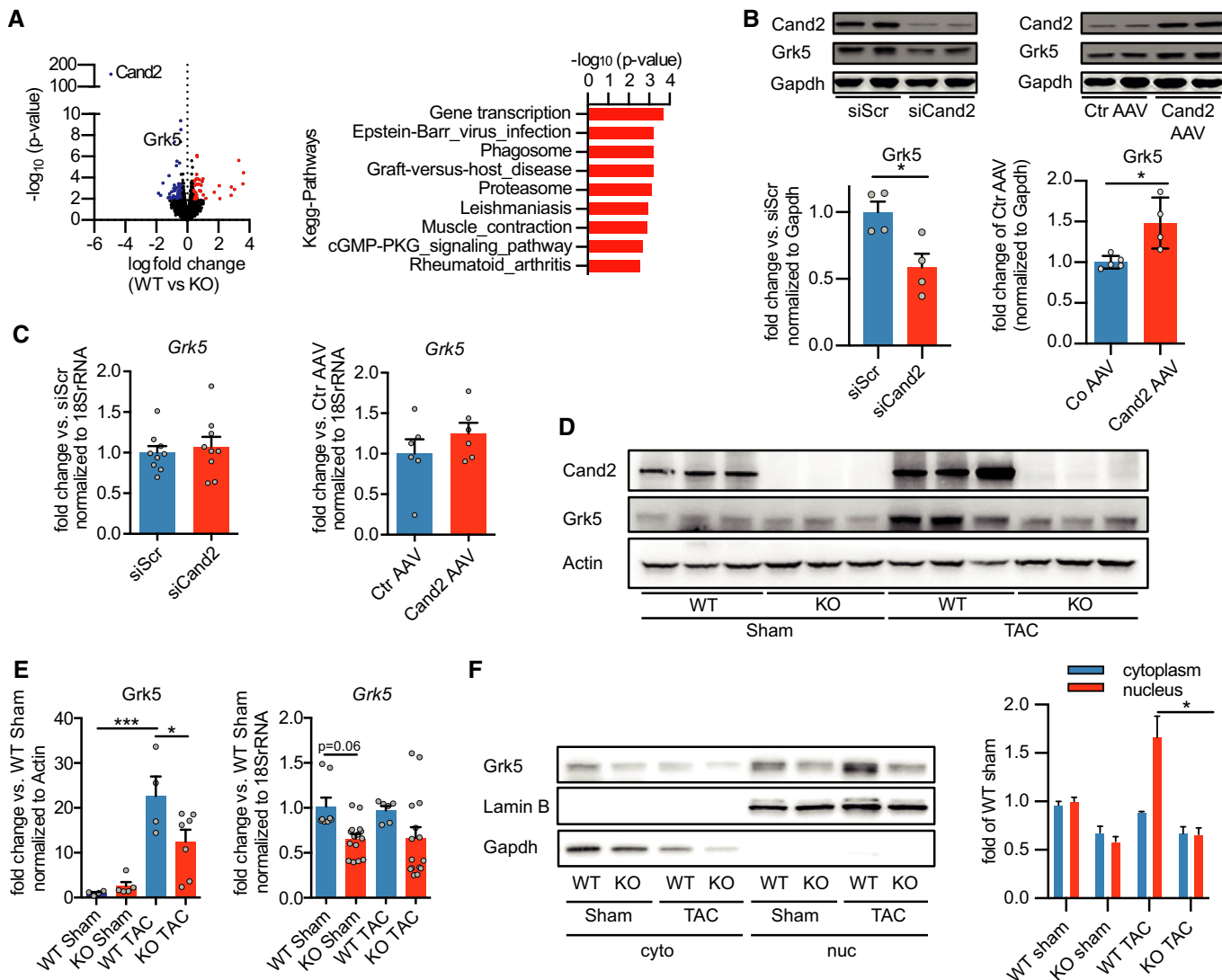


Figure 5. Cand2-dependent Grk5 expression.

- A** Volcano plot of up- ($-\log_2$ -fold change for transcripts with counts per million, CPM > 1; red dots) and downregulated ($-\log_2$ -fold change CPM < 1; blue dots) transcripts in LV after Cand2 KO. Differential expression analysis performed with edgeR; Benjamini–Hochberg method for *P*-value calculation, cutoff 0.05. Cand2 and Grk5 marked among depleted transcripts in Cand2 KO vs. WT mice. Enrichment of Kyoto Encyclopedia of Genes and Genomes (KEGG Pathways) terms for differentially expressed genes in LV of Cand2 KO vs. WT mice.
- B** Immunoblots and quantification of Grk5 protein levels *in vitro* after Cand2 KD with siRNA and after Cand2 OE with AAV6. *t*-test, *n* = 4–5 biological replicates per group.
- C** *Grk5* mRNA levels in NRCMs depleted of and overexpressing Cand2 measured by RT-qPCR. *t*-test, *n* = 6–9 biological replicates.
- D** Grk5 protein levels *in vivo* in LVs of WT and Cand2 KO mice 4 weeks after sham and TAC analyzed by immunoblotting.
- E** Quantification of Grk5 protein levels and *Grk5* mRNA levels in indicated conditions. Analyzed by one-way ANOVA, *n* = 4–15 biological replicates.
- F** Representative immunoblot of Grk5 protein levels and quantification in cytoplasmic and nuclear fractions from left ventricle lysates of WT and Cand2 KO mice after TAC surgery. Lamin B—nuclear marker, Gapdh—cytoplasmic marker. Analyzed by one-way ANOVA, *n* = 3 biological replicates.

Data information: Error bars indicate means \pm SEM. **P* \leq 0.05, ****P* \leq 0.001.

Source data are available online for this figure.

mRNAs such as *Nr4a1* and *Xirp2* (Huang *et al.*, 2006; Lehmann *et al.*, 2018) was downregulated when Cand2 was depleted both at baseline and after stimulation with PE (Fig 6B). Conversely, the levels of *Nr4a1* and *Xirp2* increased significantly in NRCMs overexpressing Cand2 (Fig 6C). Similarly, levels of *Xirp2* increased in WT mice in response to TAC but were blocked in Cand2 KO mice (Fig 6D). *In*

vitro, mTOR inhibition with Torin 1 resulted in decreased Grk5 protein levels and MEF2 luciferase activity in NRCMs, without changes in mRNA levels of *Grk5* (Fig 6E). Consistent with this, genetic activation of mTORC1 after knockdown of TSC2 resulted in increased MEF2 luciferase activity and increased Cand2 and Grk5 expression (Fig 6F).

We confirmed decreased Cand2 and Grk5 protein but not transcript levels after depletion of Raptor, the essential component of mTORC1, in cardiomyocytes (Fig 6G and H). Moreover, RT-qPCR analysis revealed downregulation of MEF2 targets such as *Nr4a1* and *Xirp2* as well as *Nppa* after knockdown of Raptor (Fig 6I), suggesting that Grk5 expression and Grk5-mediated MEF2 activity are under the direct control of mTORC1. We also tested whether adenoviral overexpression Grk5 under the condition of Raptor silencing reverses the phenotype of Raptor depletion in NRCMs (Fig 6J). Grk5 overexpression alone increased cell size as well as MEF2 targets (Fig 6K and L), but Grk5 overexpression in Raptor-depleted NRCMs only partially rescued cellular size as well as MEF2

target gene expression, suggesting that mTORC1 activity is needed for the pro-hypertrophic effect of Grk5.

Taken together, these results suggest that Cand2-dependent regulation of Grk5 levels is associated with increased MEF2 transcriptional activity, and similar to Cand2, Grk5-MEF2 is downstream of mTORC1.

Cand2 regulates Grk5 protein level by Cullin1 neddylation inhibition *in vitro*

Our findings showed that Cand2 depletion *in vitro* results in decreased Grk5 protein levels mostly independent from changes in

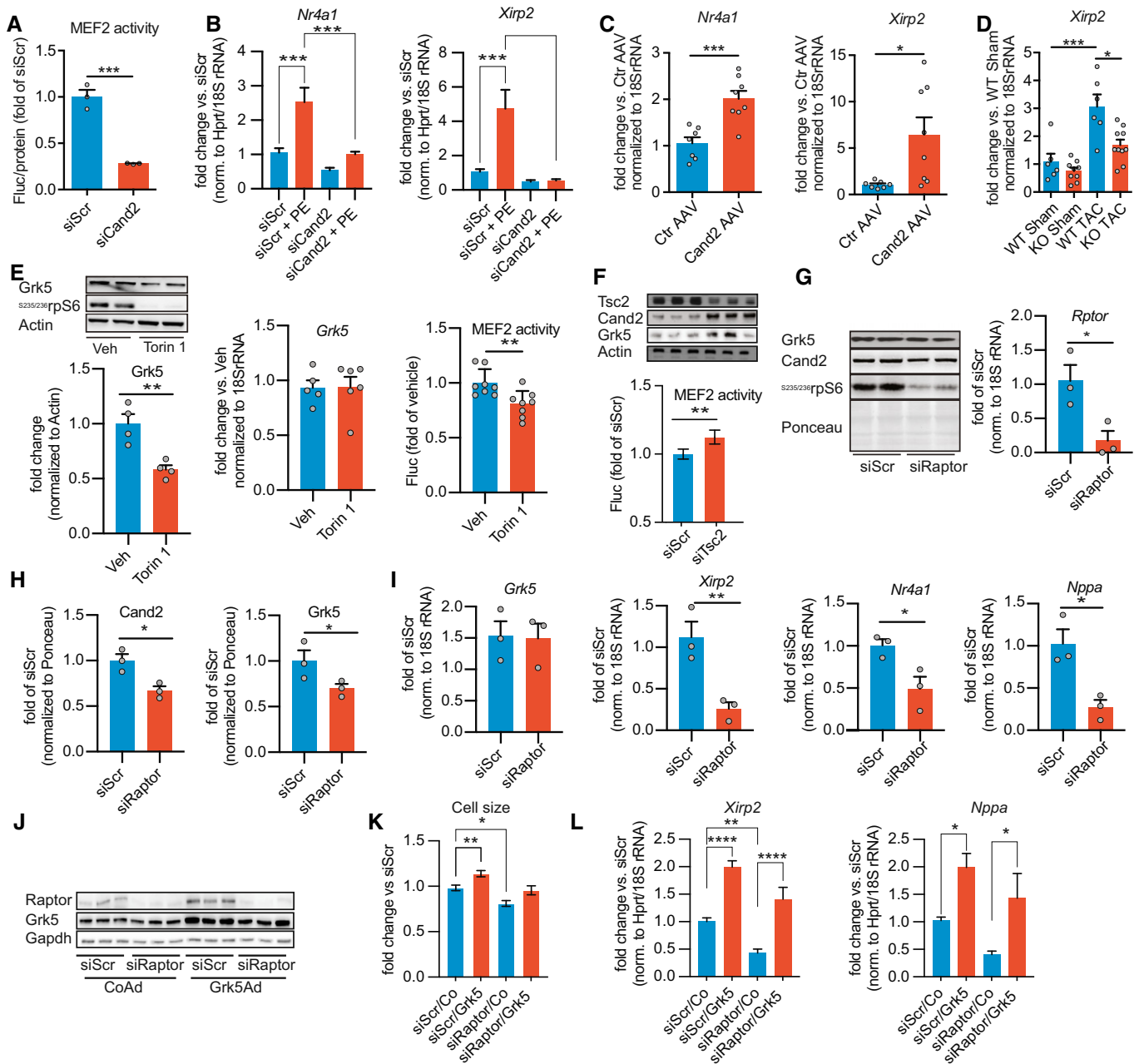


Figure 6.

Figure 6. Cand2 regulates MEF2 transcriptional activity.

- A Luciferase-based quantification of MEF2 activity after Cand2 KD in NRCMs. Analyzed by t-test, $n = 3$ biological replicates.
- B mRNA levels of MEF2-dependent genes *Nr4a1* and *Xirp2* in NRCMs with Cand2 KD for indicated groups. PE treatment for 24 h (50 μ M). Analyzed by one-way ANOVA, $n = 6$ biological replicates.
- C mRNA levels of MEF2-dependent genes *Nr4a1* and *Xirp2* in NRCMs after Cand2 OE. Analyzed by t-test, $n = 7-8$ biological replicates per conditions.
- D RT-qPCR analysis of *Xirp2* mRNA levels in LVs of WT and Cand2 KO mice after sham and TAC surgeries. Analyzed by one-way ANOVA, $n = 6-10$ biological replicates per mice group.
- E Grk5 protein and mRNA levels in NRCMs as well as MEF2 luciferase activity after 24 h of Torin 1 treatment. Analyzed by t-test, $n = 4-6$ biological replicates per conditions. Torin1 activity measured by protein levels of phosphorylated ribosomal S6 protein (^{5235/236}rpS6).
- F Cand2 and Grk5 protein levels after TSC2 KD. Analyzed by Western blot as well as MEF2 luciferase activity after TSC2 knockdown. Analyzed by t-test, $n = 5-6$ biological replicates per conditions.
- G Cand2 and Grk5 protein levels and Raptor transcript level in NRCMs after Raptor KD analyzed by Western blot. ^{5235/236}rpS6—phosphorylated ribosomal S6 protein, downstream target of mTORC1. Analyzed by t-test, $n = 3$ biological replicates.
- H Quantifications of Cand2 and Grk5 protein levels in NRCMs depleted of Raptor. Analyzed by t-test, $n = 3$ biological replicates per conditions.
- I *Grk5*, *Nppa*, and MEF2 targets *Nr4a1* and *Xirp2* mRNA levels in NRCMs after Raptor KD. Analyzed by t-test, $n = 3$ biological replicates per conditions.
- J Raptor and Grk5 protein levels after Raptor KD and adenoviral Grk5 overexpression.
- K Cell surface area measurement of NRCM for indicated groups. Analyzed by one-way ANOVA. $n = 3$ independent experiments, $n > 150$ cells.
- L RT-qPCR analysis of MEF2 targets in NRCMs after Raptor KD and Grk5 overexpression. Analyzed by one-way ANOVA. $n = 6-8$ biological replicates per conditions.

Data information: Error bars indicate means \pm SEM; * $P \leq 0.05$, ** $P \leq 0.01$, *** $P \leq 0.001$, **** $P \leq 0.0001$. Source data are available online for this figure.

transcript levels (Fig 5B), suggesting that post-transcriptional mechanisms might regulate Grk5 expression by Cand2. *In vivo*, both *Grk5* mRNA levels and protein levels are regulated by Cand2. Cand proteins modulate the activity of cullin–RING E3 ubiquitin ligases (CRLs). The activity of CRLs is dependent on cullin neddylation, whereby a covalent modification of Cul1 with the ubiquitin-like protein NEDD8 induces the conformational rearrangement of Cul1. Cand1 protein has been shown to interact with and sequester unneddylated Cul1. To find out whether Cand2, Cul1, and Grk5 directly interact in cardiomyocytes, co-immunoprecipitations were performed. Endogenous Cul1, as well as Grk5 were detected after Cand2 immunoprecipitation (IP), whereas another Cullin (Cul4) did not bind Cand2 (Fig EV4A). Additionally, we performed proximity ligation assay (PLA) in neonatal cardiomyocytes isolated from WT and Cand2 knockout mice (Fig EV4B–G). PLA signal was detected in cardiomyocytes expressing endogenous Cand2, but not in KO cells, suggesting that Cand2 is associated with Grk5 specifically. Although both proteins were observed ubiquitously in the cell, PLA signal was concentrated in the nucleus. These results support the idea that Cand2 interacts in a complex with Cul1 and Grk5.

Cand1 selectively binds to the unneddylated pool of Cul1, thereby affecting SCF ubiquitin ligase complex (Liu *et al*, 2002). Therefore, we sought to determine the effect of Cand2 on the overall neddylation status of Cullin1 in cardiomyocytes overexpressing and depleted of Cand2 (Fig 7A and B). Neddylated Cullin1 migrates slower during electrophoresis and can, therefore, be distinguished from unneddylated Cul1. Manipulation of Cand2 expression affected only the neddylated Cul1 levels, whereas the unneddylated fraction remained unchanged. The amount of neddylated Cul1 was slightly but significantly increased when Cand2 was silenced and reduced in Cand2 overexpressing cells, suggesting that Cand2 may regulate Cul1 activity (Fig 7A and B).

In line with previous reports (Zou *et al*, 2019), inhibition of neddylation by using a specific inhibitor (MLN4924) was sufficient to induce cardiomyocyte hypertrophy (Fig 7C). MLN4924 induced Cand2 protein levels independent of transcripts levels, suggesting that post-transcriptional mechanisms are responsible for increasing Cand2 protein levels (Fig EV5A). The MLN4924-induced cell growth was blocked by Cand2 knockdown, suggesting that Cand2 is

required for the increased cell size induced by MLN4924 (Fig 7C). Interestingly, we found that MLN4924-mediated inhibition of Cul1 neddylation alone was sufficient to induce an approximately 2.5-fold increase of Grk5 protein levels, independent from transcript levels measured by RT-qPCR (Fig 7D). This induction was largely attenuated after Cand2 knockdown, indicating that Cand2 is required for the induction of Grk5 after neddylation inhibition (Fig 7D). Neither Cand2 knockdown nor overexpression influenced Cul1 mRNA levels, indicating that Cand2 interacts with Cul1 on the protein level (Fig EV5B). To show that Cand2 regulates Grk5 protein stability, we assessed Grk5 half-life in cycloheximide (Cx) chase assay (Fig 7E). The Grk5 protein half-life was prolonged from approximately 18 to 27 h when Cand2 was overexpressed suggesting that Grk5 is stabilized by Cand2.

Similar to neddylation inhibition, knockdown of Cul1 increased Grk5 protein amount twofold (Fig 7F). This strongly suggests that Grk5 degradation is mediated by Cullin–RING E3 ubiquitin ligase complex. Quantitative RT-PCR analysis revealed that all changes in Grk5 levels caused by MLN4924 treatment or Cand2/Cul1 silencing resulted independently from transcriptional changes (Fig 7D–F).

To confirm that Cand2 affects cell size through Grk5, we examined whether Grk5 re-expression is sufficient to rescue the decreased cell size phenotype of Cand2-deficient cardiomyocytes. Grk5 overexpression and Cand2 depletion were confirmed by immunoblots (Fig 7G). While Cand2 knockdown reduced cellular size, Grk5 overexpression significantly increased cell size. Grk5 overexpression partly rescued the phenotype in Cand2-depleted NRCMs. In parallel, RT-qPCR analysis revealed upregulation of MEF2 targets such as *Nr4a1* and *Xirp2* after overexpression of Grk5 in Cand2-depleted cells (Fig 7H). Conversely, Grk5 knockdown in the presence of Cand2 overexpression blocked the hypertrophic cell growth induced by Cand2 (Fig 7I). RT-qPCR analysis revealed upregulation of direct MEF2 targets such as *Nr4a1* and *Xirp2* after overexpression of Cand2 which was reversible after Grk5 knockdown (Fig 7J), suggesting that Grk5 signaling is downstream of Cand2 *in vitro*. Furthermore, we tested whether overexpression of MEF2 could rescue the effect of Cand2 silencing (Fig EV5D–E). Adenoviral overexpression of MEF2c in NRCMs resulted in increased expression of

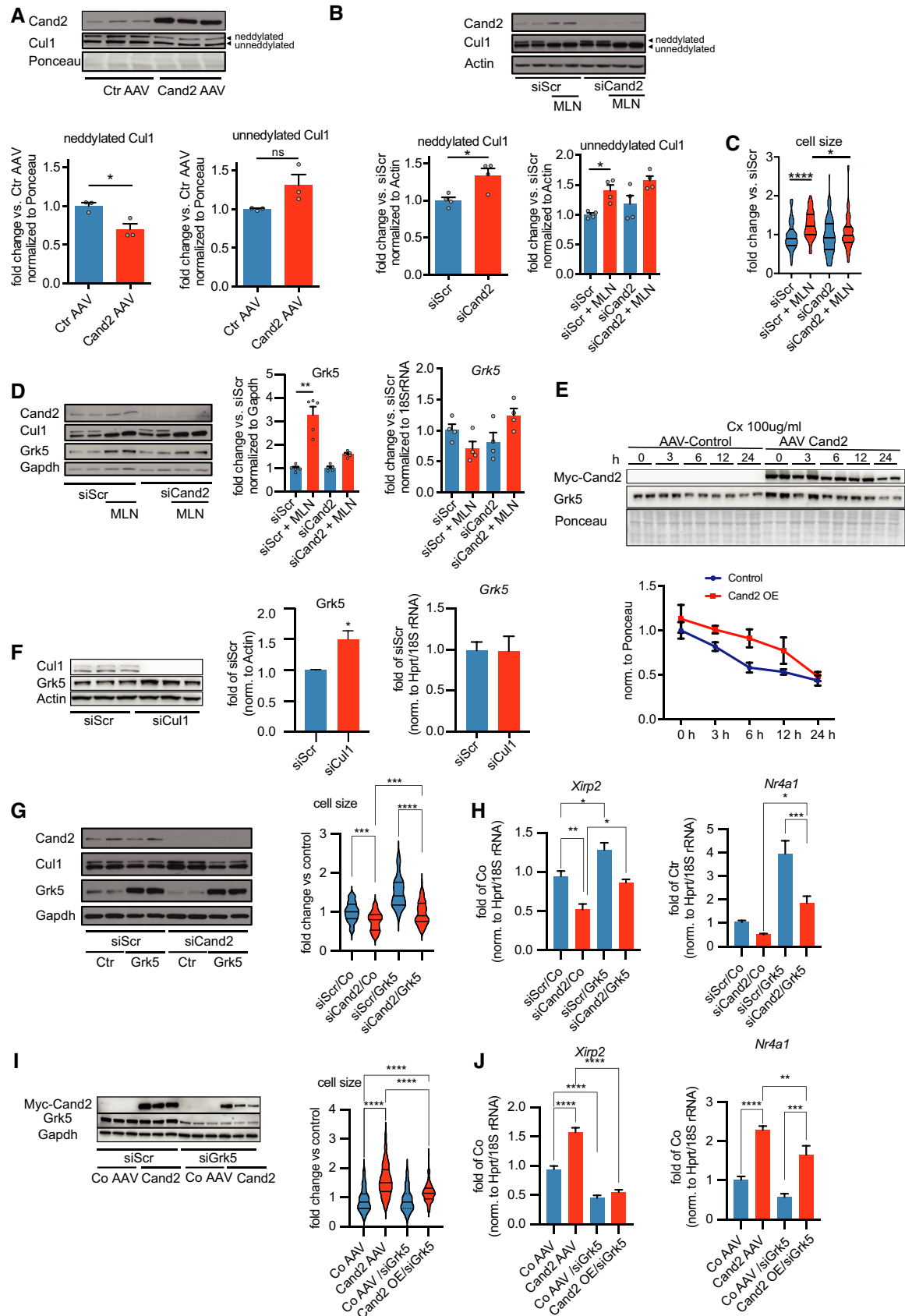


Figure 7.

Figure 7. Cand2 and Cullin1 neddylation modulate Grk5 protein level.

- A Representative immunoblot and its quantification of protein levels of neddylated and unneddylated Cul1 in NRCMs after Cand2 overexpression. Analyzed by *t*-test, *n* = 3 biological replicates per conditions.
- B Cul1 neddylation analyzed by Western blot in NRCMs depleted of Cand2. NRCMs were treated with MLN4924 (100 nM) to block Cul1 neddylation. Quantification of neddylated and unneddylated Cul1 protein levels after MLN4924 treatment for 24 h. *t*-test, *n* = 4 biological replicates.
- C Cell size area measurement of NRCMs after Cand2 KD and neddylation inhibition (MLN). Analyzed by one-way ANOVA. *n* = 3 independent experiments with > 150 cells. Violin plot: the middle horizontal lane—median, upper lane—3rd quartile, lower lane—1st quartile.
- D Grk5 expression in NRCMs upon Cand2 KD and Cul1 neddylation inhibition (MLN) analyzed by immunoblot and RT-qPCR. Analyzed by one-way ANOVA, *n* = 4–5 biological replicates.
- E The half-life of Grk5 in HeLa cells overexpressing Cand2 measured by cycloheximide chase. *n* = 2 biological replicates.
- F Representative immunoblot and quantification of Grk5 protein levels as well as quantification of mRNA levels after Cul1 KD. *t*-test, *n* = 4 biological replicates.
- G Immunoblot after Cand2 KD and Grk5 OE. Cell surface area measurement of NRCM for indicated groups. Analyzed by one-way ANOVA. *n* = 3 independent experiments with > 150 cells. The middle horizontal lane on violin plot—median, upper lane—3rd quartile, lower—1st quartile.
- H mRNA levels of MEF2-dependent genes *Nr4a1* and *Xirp2* in NRCMs for indicated groups. Analyzed by one-way ANOVA, *n* = 6 biological replicates.
- I Immunoblot after Cand2 OE and Grk5 knockdown. Cell surface area measurement of NRCM for indicated groups. Analyzed by one-way ANOVA. *n* = 3 independent experiments with >150 cells. The middle horizontal lane on violin plot—median, upper lane—3rd quartile, lower—1st quartile.
- J mRNA levels of MEF2-dependent genes *Nr4a1* and *Xirp2* in NRCMs for indicated groups. Analyzed by one-way ANOVA. *n* = 6 biological replicates.
- Data information: Error bars indicate means ± SEM; **P* ≤ 0.05, ***P* ≤ 0.01, ****P* ≤ 0.001, *****P* ≤ 0.0001.
Source data are available online for this figure.

MEF2 target genes, as well as increased cell size. MEF2c overexpression also induced target genes in Cand2-depleted cells but was not sufficient to increase cell size in Cand2-depleted cells, suggesting that Cand2 regulates cellular growth also *via* additional pathways.

Cand2 knockout results in decreased hypertrophic remodeling early after TAC

Since Cand2 expression is induced early after TAC, we examined early pathological remodeling 2 days after TAC surgery in Cand2 KO mice compared to WT mice. Cand2 KO mice along WT littermates were subjected to TAC or sham surgery and phenotypic consequences were analyzed 2 days after surgery. TAC-induced *Nppa* and *Nppb* levels as well as induction of MEF2 target genes *Xirp1* and *Nr4a1* in WT mice were significantly reduced in Cand2 KO mice (Fig 8A). TAC surgery resulted in an increased LV/BW ratio in WT mice (Fig 8B). In contrast, Cand2-deficient mice showed a significantly decreased LV/BW ratio compared to TAC-operated WT mice. Early cardiac remodeling was associated with increased Grk5 protein levels in WT mice, which was predominantly regulated at the protein levels since Grk5 mRNA levels were not significantly increased in TAC-operated mice compared to sham-operated animals. Induction of Grk5 was blocked in Cand2 KO mice (Fig 8C). In line with our observation *in vitro*, Cand2 depletion resulted in higher levels of neddylated Cul1 (Fig 8D). Taken together, we suggest a novel myocyte-specific and mTORC1-mediated signaling cascade. mTORC1-dependent control of Cand2 expression results in activation of the pro-hypertrophic Grk5-MEF2 axis *via* post-transcriptional regulation of Grk5 protein levels by the Cul1-SCF ubiquitin ligase complex (Fig 8E).

Discussion

This study provides evidence for a novel role of Cand2, a component of the SCF (SKP1-Cul1-F-box protein) E3 ubiquitin ligase complex, in the myocardium. Cand2 is a muscle-specific protein that we identified in a cardiomyocyte genome-wide screen for mTORC1-dependent gene expression control at the level of mRNA translation. Several studies and our work showed that mTORC1-signaling

controls physiological and pathological myocardial remodeling (Völkens *et al*, 2013, 2014; Sciarretta *et al*, 2018). The central role of mTORC1 in integrating multiple intra- and extracellular parameters requires an elaborate control system to accomplish fine-tuning of signaling to downstream targets. Clinically, targeting mTORC1 with rapamycin is already an established application to prevent re-stenosis after percutaneous coronary stent implantation. Systemic pharmacological or genetic mTORC1 inhibition prevented pathological hypertrophy and improved cardiac function in murine disease models (Shioi *et al*, 2003; Buss *et al*, 2009; Völkens *et al*, 2013). Still, the identity of mTORC1 translationally regulated mRNAs in the diseased heart was largely unknown. We identified several mTOR-dependent genes *in vitro* and characterized Cand2 in follow-up experiments. Given the complexity of mTORC1-dependent signaling in response to stress, Cand2 upregulation is definitely only one of many effectors downstream of mTOR that regulate cardiac remodeling.

Cand2 is a translationally upregulated gene dependent on the activity of mTORC1 during pathological stress both *in vitro* and *in vivo*. We found that Cand2 is required for pathological hypertrophy in cardiomyocytes. Cand2 KO mice were protected against pathological remodeling and cardiac dysfunction, which was associated with reduced levels of Grk5 and MEF2-dependent gene expression profiles. Conversely, overexpression of Cand2 was sufficient to drive pathological hypertrophy and gene expression *in vitro*. Cand2 expression was also found to be upregulated in human cardiomyopathy patients (van Heesch *et al*, 2019).

Cand2 was initially identified as a muscle-specific homolog of Cand1 and its only described function was the acceleration of myogenesis in skeletal myoblasts during differentiation (Aoki *et al*, 1999; Shiraishi *et al*, 2007). Interestingly, Cand2 has been linked to atrial fibrillation susceptibility using expression quantitative trait loci mapping. Increased levels of Cand2 correlated with a higher incidence of atrial fibrillation (Sinner *et al*, 2014; Wei *et al*, 2016; Gregers *et al*, 2017), suggesting that Cand2 might drive pathological remodeling in the atrium.

Mechanistically, Cand proteins modulate the activity of Cullin-RING E3 ubiquitin ligases (CRLs). The substrate-binding domain of Cullins, through their adaptors, can recruit hundreds of known substrate receptors that specifically target an even larger array of

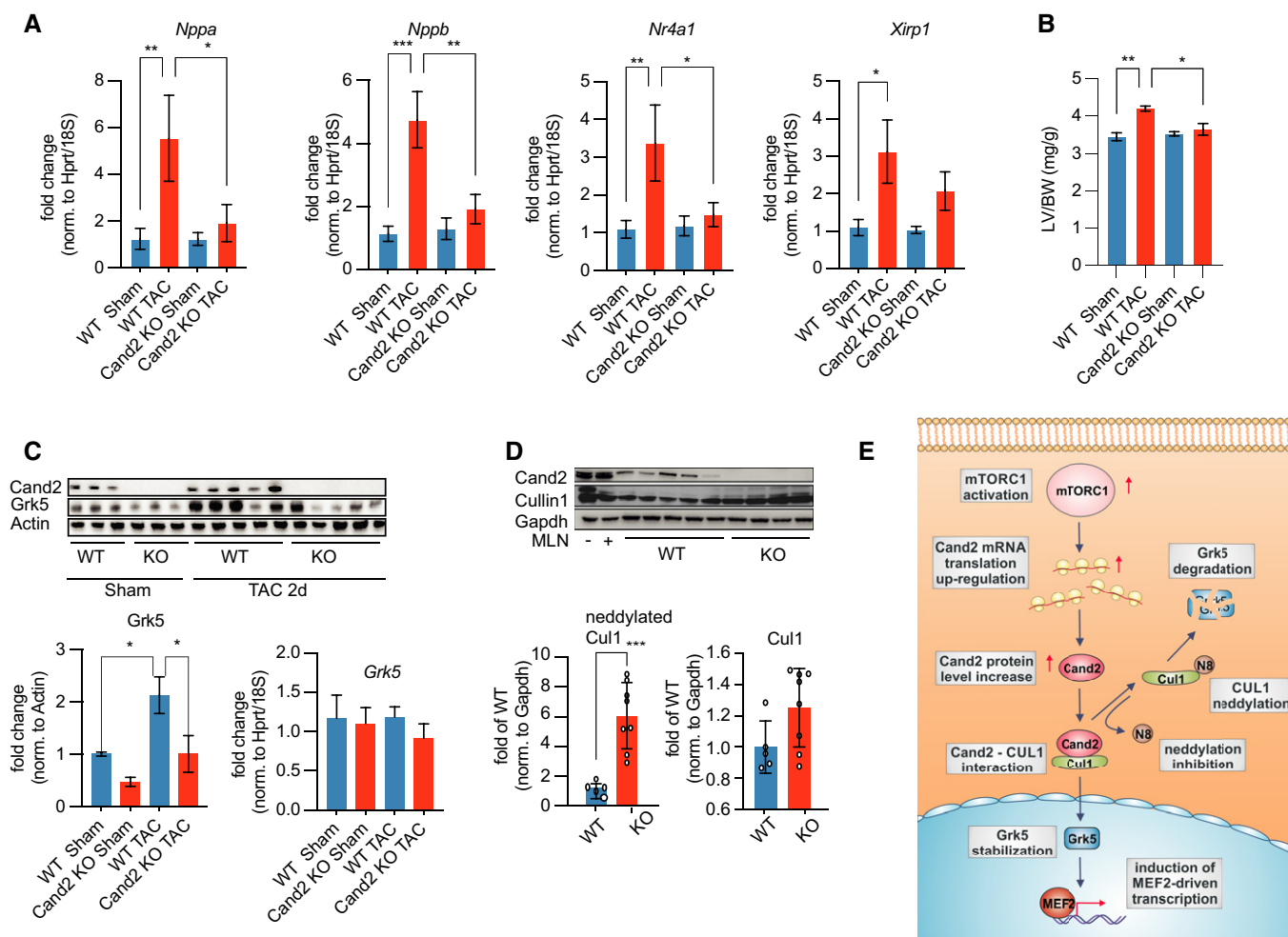


Figure 8. Cand2 regulates Grk5 levels *in vivo* after TAC.

- A Quantification of indicated mRNA levels 2 days after TAC measured by RT-qPCR. Analyzed by one-way ANOVA. $n = 5-7$ biological replicates per group.
- B LV weight to body weight ratio (mg/g) of WT and Cand2 KO mice subjected to sham and TAC surgeries after 2 days. Analyzed by one-way ANOVA. $n = 5-7$ biological replicates per group.
- C Grk5 protein levels *in vivo* in LVs of WT and Cand2 KO mice 2 days after sham and TAC analyzed by immunoblotting as well as quantification of mRNA levels analyzed by RT-qPCR. Analyzed by One-way ANOVA. $n = 3-5$ biological replicates per group.
- D Representative immunoblot and its quantification of protein levels of neddylated and unnedylated Cul1 in Cand2 KO mice compared to WT mice. Analyzed by t-test. $n = 5-8$ mice per group. Cul1 neddylated was inhibited in C2C12 (-/+ MLN) for neddylated Cul1 band detection.
- E Model of Cand2-dependent stabilization of Grk5 by Cul1 neddylation inhibition in mTOR-dependent manner.

Data information: Error bars indicate means \pm SEM; * $P \leq 0.05$, ** $P \leq 0.01$, *** $P \leq 0.001$.

Source data are available online for this figure.

substrates. It has become increasingly evident that the cardiac ubiquitin-proteasomal function is not only highly dynamic but is also critical for healthy myocardium (Drews & Taegtmeier, 2014). Just as CRLs regulate protein levels and function by covalent modification, they are subjected to posttranslational modifications regulating ligase activity. A ubiquitin-like protein NEDD8, is covalently attached to a conserved lysine residue in the C-terminal Cullin homology domain. The activity of CRLs is largely dependent on Cullin neddylation, whereby NEDD8 induces conformational rearrangement of Cullins. Cand proteins have been shown to interact with and sequester unnedylated Cullins (Liu *et al*, 2018). Thus, Cand proteins have been initially characterized as inhibitors of

NEDD8 conjugation, which initially implied that Cand proteins are negative regulators of CRLs. However, subsequent studies of Cand1-deficient cells and organisms suggested also a positive regulatory function of Cand on CRLs (Liu *et al*, 2018). Importantly, neddylation homeostasis is crucial for the integrity of the heart. Complete loss of neddylation in cardiac myocytes resulted in dilated cardiomyopathy with premature death (Su *et al*, 2011, 2013). Pharmacological inhibition of neddylation using a selective neddylation inhibitor MLN4924 promoted pathological hypertrophy and resulted in cardiac failure (Zou *et al*, 2018, 2019).

Neddylation of Cullins can provide a regulatory mechanism that fine-tunes substrate ubiquitination and targeting for proteasomal

degradation. We found that in response to stress such as pressure overload, Cand2 regulates expression of Grk5 predominantly independently of the transcript levels. However, Grk5 mRNA levels are decreased in Cand2 KO mice, suggesting that additional mechanisms involving regulation of Grk5 transcription exist in the Cand2 KO mice. Previous work showed that following pressure overload, Grk5 accumulated in the nucleus of cardiomyocytes and acts in the nucleus as a class II histone deacetylase (HDAC) kinase, phosphorylating specifically HDAC5 leading to its nuclear export and repression of the transcription factor MEF2 as well as NFAT (Cannavo *et al*, 2016; Traynham *et al*, 2016). Furthermore, transgenic mice with Grk5 cardiac overexpression could not cope with pressure overload (Martini *et al*, 2008). Once free of repression, MEF2 and NFAT are responsible for the transcription of hypertrophic genes, leading to pathological hypertrophy (Zhang *et al*, 2011).

Our study showed that reduced levels of Grk5 in Cand2-depleted myocytes resulted in decreased MEF2 activity. We also confirmed the direct interaction of Cand2 with Cul1 and Grk5 in myocytes, supporting the hypothesis that Cand2 controls Cul1-dependent Grk5 levels in cardiomyocytes. Moreover, pharmacological inhibition of neddylation using a selective neddylation inhibitor MLN4924 resulted in the loss of Cul1 neddylation and increased cell size, which was associated with increased Grk5 levels independent from transcript levels. Cardiomyocytes depleted of Cand2 did not respond to MLN4924, suggesting that Cand2 is necessary for growth induction caused by MLN4924. Rescue of Grk5 expression in Cand2-depleted cells reversed the observed phenotype with increased pathological cell size similar to control cells.

Taken together, we suggest a mechanism by which pathological mTORC1 signaling links translationally controlled Cand2 expression to transcriptional activity. We suggest that these findings might be transferable toward novel treatment options. We hypothesize that Cand2 is a promising target as it is a cardiac muscle-specific protein, early (translationally) upregulated during disease initiation, and sufficient for pathological remodeling. Future studies will develop a nucleic acid-based therapy against Cand2. Recent advances in nucleic acid-based therapeutics show promising results in treatments for various diseases including pathological cardiac hypertrophy and it should be possible to target Cand2 translation by antisense oligonucleotides targeting the 5' UTR of Cand2 (Moriyama *et al*, 2017). Future studies are also needed to identify additional interaction partners of Cand2 dependent on the neddylation status of Cul1 to understand how mTORC1-dependent upregulation of Cand2 affects the stability of protein networks in the nucleus.

Materials and Methods

The authors declare that all supporting data are available within the article (and in the Dataset EV1 and Dataset EV2).

Parallel generation of Ribo-seq and RNA-seq libraries

Ribo-seq and RNA-seq libraries were prepared for each biological replicate. Ribosome footprints were generated after immunoprecipitation of cardiomyocyte-specific monosomes with anti-HA magnetic beads after treating the lysate with RNase I. Libraries were generated according to the mammalian Ribo-seq kit (Illumina). Barcodes

were used to perform multiplex sequencing and create sequencing pools containing at least eight different samples and an equal amount of RNA and RPF (Ribosomal Protected Fragment) libraries. Sample pools were sequenced on the HiSeq 2500 platform using 50-bp sequencing chemistry.

The Ribo-Taq mouse model and ribosome-protected fragments immunoprecipitation were described previously (Doroudgar *et al*, 2019). To identify mTOR-dependent translatoome *in vitro* polysome fractions from NRCMs were isolated in a sucrose gradient according to standard procedure (Kmietczyk *et al*, 2019). Absorbance was monitored at 254 nm to record the polysome profile. The collected fractions were treated with RNaseI and mixed with Qiazol to recover ribosomal footprints. Generation of Ribo- and RNA-seq libraries and deep-sequencing data processing were described in detail (Doroudgar *et al*, 2019). Briefly, 15 million NRCMs were lysed in 500 μ l poly-some buffer (20 mM Tris pH 7.4, 10 mM MgCl₂, 200 mM KCl, 2 mM DTT, 100 μ g/ml CHX, 1% Triton X-100, 1 U DNase/ μ l) containing 100 μ g/ml CHX. The lysate was used for RPF generation using polysome profiles after RNase I digestion. For complete lysis, the samples were kept on ice for 10 min and subsequently centrifuged at 20,000 g to precipitate cell debris and the supernatant was immediately used in the further steps. Sucrose solutions were prepared in polysome gradient buffer and 20 U/ml SUPERase-In (Ambion). Sucrose density gradients (10–50% wt/vol) were freshly made in SW40 ultracentrifuge tube using a BioComp Gradient Master (BioComp). Ribosome footprints were generated after treating the lysate with RNase I (Ambion). Cell lysates were loaded onto sucrose gradients, followed by centrifugation for 250 min at 220,000 g, 4°C, in an SW40 rotor. Separated samples were fractionated at 0.375 ml/min by using a fractionation system BioComp Gradient Station (BioComp) that continually monitors OD254 values. Monosomal fractions were collected into tubes at 0.3-mm intervals. Libraries were generated according to the mammalian Ribo-seq kit (Illumina). Sample pools were sequenced on the HiSeq 2000 platform using 50-bp sequencing chemistry.

Data analysis and visualization

For RNA-Seq R and Bioconductor were used with the NGS analysis package systempipeR (Backman & Girke, 2016). Quality control of raw sequencing reads was performed using FastQC. Low-quality reads were removed using trim_galore (version 0.6.4). The resulting reads were aligned to the mouse genome version mm10 from UCSC using tophat2 (Kim *et al*, 2013). EdgeR (version 3.26.8) was used to perform a differential expression analysis (Robinson *et al*, 2010). A false-positive rate of $\alpha = 0.05$ with FDR correction was taken as the level of significance. Volcano plots were created using R (version 3.4.0) using the ggplot2 package (version 2.2.1).

For Ribo-seq data, only periodic fragment lengths were kept that showed a distinctive triplet periodicity. We used the automatic Bayesian selection of read lengths and ribosome P-site offsets (BPPS) method (Malone *et al*, 2016) to select and shift aligned reads to properly account for the P-site of the ribosome. We only considered data points with read count observations across all replicates. We used $\log_2FC > 1.5$ as a cutoff. For myocytes data, we did not estimate significance but provide only fold change values due to the absence of biological replicates.

GO-term enrichment analysis was performed using DAVID (Database for Annotation, Visualization and Integrated Discovery) with

the rat genome as background. Only enriched GO terms with at least three significantly changed genes were kept for further analysis and ranked by Fisher Exact. Top enriched terms were retained and visualized with a custom plotting routine showing enrichment p-value.

Mice, surgery, and cardiac function

To study *Cand2* *in vivo*, a novel *Cand2* knockout mouse line was created. An embryonic stem cell clone (EPD0169_1_A01-European Conditional Mouse Mutagenesis Program) was used to generate *Cand2* knockout mice. At 8 weeks of age, male *Cand2*^{-/-} mice underwent transverse aortic constriction (TAC; 27-gauge needle) or sham operation, as previously described (Kmietczyk *et al.*, 2019). Institutional Animal Care and Use Committee approval was obtained for all animal studies. For Torin 1 injection, 25 mg/ml Torin 1 was dissolved in 100% N-methyl-2-pyrrolidone and diluted 1:4 in 50% PEG400 before injection. Mice were injected twice a day with 10 mg/kg for 2 days.

Isolation and primary cell culture

Ventricular cardiomyocytes from 1- to 2-day-old Wistar neonatal rat hearts (NRCMs) were prepared by trypsin digestion and percoll gradient separation according to standard procedures (Sanjalp *et al.*, 2020). Simultaneously, ventricular fibroblasts were obtained. For analysis of hypertrophy, cells were treated with 50 μ M PE for indicated time points. mTORC1 was pharmacologically inhibited with 100 nM Torin 1 for indicated time points. For generation of the Ribo-Seq libraries, mTORC1 was pharmacologically inhibited with 100 nM Torin 1 for 3 h. For neddylation inhibition, NRCMs were treated with 100 nM MLN4924 for 24 h. Neonatal mouse heart myocytes were isolated from 1-day-old wild-type and *Cand2* knockout mice by DNaseI/collagenase type III digestion according to the published protocol (Ehler *et al.*, 2013).

Adult ventricular cardiomyocytes were isolated using standard procedures as previously described (Kmietczyk *et al.*, 2019). Cardiac endothelial cells were isolated from 7- to 12-day-old murine hearts. After heparin injection, hearts were removed and left ventricles were separated and homogenized by collagenaseI/DNaseI digestion. Endothelial cells were isolated by rotation with CD31 coated DynaBeads (sheep anti-rat IgG, Invitrogen) for 45 min at 37°C in 5% CO₂. After the first passage, cells were additionally purified by pull-down with CD120 coupled DynaBeads.

Plasmids and overexpressions

5' TOP-reporter constructs were obtained by cloning of *Cand2*, eEF2, and β -Actin 5'UTRs into piCheck2 plasmid upstream of Renilla luciferase. HEK cells were transfected with 5'UTR-reporters for 24 h using ViaFect reagent according to the manufacturer's protocol (Promega). Next, HEK cells were treated with 250 nM Torin 1 for 6 h. *Cand2* overexpression *in vitro* was obtained by NRCMs transduction with AAV6 vector. Mouse *Cand2* (NM_025958.2) containing Myc-tag inserted after START codon was chemically synthesized (BioCat) and cloned into recipient vector pSSV9. To determine the optimal MOI, a preliminary dose-escalation experiment was conducted with different doses of *Cand2* AAV6. For MEF2 and Grk5 studies, NRCMs were infected with adenoviruses harboring 3xMEF-luc (Firefly luciferase; a gift from Prof. Johannes Backs), mouse HA-

tagged MEF2c (pcDNA3.1-MEF2C-HA plasmid was a gift from Prof. Andrew Lassar, Addgene #32515), and bovine Grk5 (gift from Prof. Philip Raake) for 24 h.

RNA interference

Pre-designed synthetic anti-rat *Cand2* small interfering RNA (siRNA ID s140407), anti-Cul1 siRNA (s168977), anti-Rptor siRNA (s143005), anti-Grk5 siRNA (s222052), anti-TSC2 siRNA (s200189), and scrambled siRNA (Silencer™ Select Negative Control No. 1 siRNA) as negative control were purchased in Thermo Fisher Scientific. NRCMs were transfected with 25 nM final concentration of siRNAs by using HiPerfect transfection reagent according to the manufacturer's instructions (QIAGEN).

RNA isolation and RT-qPCR

Total RNA from NRCMs was isolated with Quick-RNA™ MiniPrep (Zymo Research) according to the manufacturer's protocol. Liquid nitrogen snap-frozen tissues were homogenized in Precellys 24 homogenizer (Bertin Instruments) in 500 μ l of lysis buffer containing 20 mM Hepes pH 7.4-7.5, 10 mM MgCl₂, 200 mM KCl, 1% Triton, 1 \times protease inhibitor, 1 \times phosphatase inhibitor, 25 U/ μ l DNase I, and 40 U of RNasin. A 100 μ l aliquot was mixed with 1 ml of Qiazol to isolate total RNA according to the standard protocols with chloroform and isopropanol precipitation. The quality of total RNA was checked on a NanoChip 2100 Bioanalyzer (Agilent). 100–500 ng of total RNA was reverse-transcribed into complementary DNA (cDNA) by using iScript™ Reverse Transcription Supermix (Bio-Rad). Quantitative real-time PCR was performed using iTAQ™ SYBR Green PCR Kit (Bio-Rad) according to the manufacturer's instructions. Primers used in the study are shown in Table 1. Analysis of the specificity of the amplification product was performed by melting curve analysis. We calculated quantitative differences using the $\Delta\Delta C(T)$ method.

Immunoblots

Samples were combined with the appropriately concentrated form of Laemmli sample buffer and then boiled before SDS-PAGE followed by transfer to PVDF membranes.

A list of all used antibodies is provided in Table 2.

Histology, immunohistochemistry, and PLA

Sections were cut and deparaffinized using standard procedures. In brief, hearts were excised and embedded in formalin for 24 h at room temperature. After cutting, sections were deparaffinized and rehydrated, and antigens were *retrieved*.

NRCMs and ARCMs were plated on permanox or glass chamber slides (gelatin coated) and fixed by paraformaldehyde, permeabilized, and blocked as described (Völkens *et al.*, 2013). *Cand2* primary antibody (Bethyl Laboratories) diluted 1:100 vol/vol in the respective blocking solution was applied to both types of slides overnight at 4°C. *Cand2* was detected by FITC or Cy3-conjugated secondary antibody (Jackson Laboratories). Alexa Fluor™ 555 Phalloidin (Thermo Fisher Scientific) or conjugated phalloidin 633 (Jackson Laboratories) was used to detect F-actin. DAPI (Life Technologies)

Table 1. List of primers.

Gene	Forward (5'–3')	Reverse (5'–3')
Rat Nppa	TACAGTGGCGTGCCAACACAGAT	TGGGCTCAATCCTGTCAATCCTA
Rat Nppb	GAACAATCCATGATGCAGAAGC	GCTGTCTCTGAGCCATTTCTT
Rat Grk5	CTCTTCAGGCGTCAGCATCA	AGGCCAGAGCTGAAACTAGC
Rat Cand2	CAAAGACTTCAGGTTTATGGCTAC	GTTCTGCACCTCACCCTCC
Rat Cand1	TGGAAGATGGTTTGAAGGACCA	ACAGAGTTCCGCCCTTACCTTA
Rat Nr4a1	CTTCAAACCCAAGCAGCCC	CTTCAAACCCAAGCAGCCC
Rat Xirp2	TCGCCTACAAACCTCAGACG	ACAGTTTCACTCAAAAAGGCCAA
Rat Raptor	AGAGCTGGAGAATGAAGGATCG	AGGACCATAGACAGAGGATCAAT
Rat, mouse HPRT	GGGGCTGTACTGCTTAACCAG	TCAGTCAACGGGGGACATAAA
Mouse Cand2	GGGCAAGGTGAAGGAGTACC	TGGTGTGTTGGCTGTGATC
Rat, mouse 18S rRNA	CGAGCCGCTGGATACC	CATGGCCTCAGTTCCGAAAA
Mouse Grk5	CTCCGAAGGACCATAGACAGAG	CGCCCCAAGGTTTTCATCTG
Mouse Xirp2	GCAGCTTCTCGGCTAATGTCA	CTCAGAAAAGGCGTTGCAGG
Mouse Nr4a1	GTGCAGTCTGTGGTACAATGC	CAGGCAGATGTACTTGGCGCTT
Mouse Nppa	TTGTGGTGTGTACCGAGCT	TGTTACCACGCCACAGTG
Mouse Nppb	TTTGGGCTGTAACGCACTG	CACTTCAAAGGTGGTCCCAGA
Mouse Cand1	GACGACGATGACCAAGGGAG	TAACACAGCGTCCAGGCAC
Mouse Desmin	AGTGCATGAAGAGGAGATCCG	GTTCTTAGCCGGATGGTCT
Mouse 4EBP1	ACTCACCTGTGGCCAAAACA	TTGTGACTTTCACCCGCTG
Bovine Grk5	CTGTTAGACGATTACGGCCACA	GGAGCCATGTAGCCAACGG
Mouse MEF2c	CCCACGCACTGAAGAAAAAT	ACTGTTGTGGCTGGCACTG
Mouse rp55	GCGCCCTCAGGATGACTG	GGCATACTTCTCTTACAGCA
Mouse rpS20	AAAGATAACCGGAAAGACGCC	AGTCCGCACAAACCTTCTCC
Mouse eEf2	CTGTGTCTGTCCAAGTCCCC	TACTTTTCGGCCAGGGTAGCG

was diluted in Vectashield (Vectra Labs) mounting media and used as nuclear staining.

Proximity ligation assay was performed according to the manufacturer's instructions (DuoLink in situ red kit Mouse/Rabbit) in rat and mouse neonatal cardiomyocytes. Primary antibodies were diluted 1:20 in DuoLink antibody diluent and incubated with cells at 4°C overnight. For Cand2-Grk5 detection, anti-rabbit TIP120B and anti-mouse Grk5 were used. For Cand2-Cul1 anti-mouse TIP120B and anti-rabbit Cul1 antibodies were applied. The connective tissue was visualized with WGA Alexa Fluor™ 488 conjugate (Thermo Fisher Scientific). Images were obtained with 20× and 60× objectives.

Immunoprecipitation

NRCMs were treated with 1 μM MLN 4924 for 6 h and lysed with ice-cold IP lysis buffer containing 40 mM Hepes pH 7.4, 2 mM EDTA, 10 mM sodium pyrophosphate, 10 mM glycerophosphate, and 0.3% CHAPS. M280 sheep anti-rabbit Dynabeads were coated with anti-rabbit TIP120B antibody in IP lysis buffer for 1 h at room temperature. 500 μg of protein lysate was combined with antibody-coated beads and rotated at 4°C overnight. Beads were washed three times with IP lysis buffer supplemented with 150 mM NaCl. Immunocomplexes were eluted with SDS sample buffer by boiling

for 5 min, and proteins were detected by immunoblotting with a corresponding antibody.

Subcellular fractionation

Subcellular fractionation of left ventricles was performed as previously described with small modifications (Wysocka *et al*, 2001). Briefly, hearts were washed with ice-cold PBS and homogenized in buffer A (10 mM Hepes pH 7.9, 10 mM KCl, 1.5 mM MgCl₂, 340 mM sucrose, 10% glycerol, 1 mM DTT, 1x proteases inhibitor cocktails, 1X Triton) with tight-fitting disposable tissue grinder pestle and needled with 20- and 22-gauge needles. Nuclear pellets and cytoplasmic supernatants were separated by low-speed centrifugation at 1,300 g, 4°C for 5 min. The final cytoplasmic fraction was pre-cleared by high-speed centrifugation at 20,000 g for 5 min at 4°C. The nuclear pellet from low-speed centrifugation was dissolved in the hypotonic buffer B containing 3 mM EDTA, 0.2 mM EGTA, 1 mM DTT, 1x proteases inhibitor cocktails.

Luciferase assays

Cells were harvested 24–48 h after transfection/infection in passive lysis buffer (Promega). The samples were prepared according to the manufacturer's protocol (Promega) and measured by using a

Table 2. List of primary antibodies.

Antigen	Primary antibody	Origin	Company	Cat.#	Application
Cand2	TIP120B	Rabbit	Bethyl Laboratories	A304-046A-M	WB, IP, IF, PLA
Cand2	TIP120B (H7)	Mouse	Santa Cruz	sc-515406	WB, PLA
Grk5	Grk5 (D9)	Mouse	Santa Cruz	sc-518005	WB, PLA
Cul1	Cul1 (D5)	Mouse	Santa Cruz	sc-17775	WB, PLA
Cul1	Cul1	Rabbit	Bethyl Laboratories	A303-373A-M	WB, PLA
Cand1	TIP120A (G-3)	Mouse	Santa Cruz	sc-137055	WB
GAPDH	GAPDH (G9)	Mouse	Santa Cruz	sc-365062	WB
β-Actin	Beta-Actin (C4)	Mouse	Santa Cruz	sc-47778	WB
prpS6	pS6RP (Ser235/236)	Rabbit	Cell Signaling	4858S	WB
p4E-BP1	p4E-BP1 (Ser65)	Rabbit	Cell Signaling	9451S	WB
4E-BP1 T37/46	Phospho-4E-BP1 (Thr37/46)	Rabbit	Cell Signaling	2855S	WB
4E-BP	4E-BP	Rabbit	Cell Signaling	9452	WB
S6K1 T389	Phospho-p70 S6 Kinase (Thr389)	Rabbit	Cell Signaling	9205L	WB
pERK 1/2	Thr218/Tyr220	Rabbit	Cell Signaling	3371	WB
Mapk (T202/204)	Phospho-p44/42 MAPK (Erk1/2) (Thr202/Tyr204)	Rabbit	Cell Signaling	9101	WB
p38 (T180/182)	Phospho-p38 MAPK (Thr180/Tyr182) (12F8)	Rabbit	Cell Signaling	4631	WB
Myc-Tag	(71D10)	Rabbit	Cell Signaling	2278S	WB
pAkt1	Ser473	Rabbit	Cell Signaling	9271	WB
Csq	calsequestrin	Rabbit	Abcam	Ab3516	WB
rpS6	S6 Ribosomal Protein (5G10)	Rabbit	Cell Signaling	2217	WB
rpS5	rpS5	Rabbit	Abcam	Ab210745	WB
Lamin B1	Lamin B1 (B10)	Mouse	Santa Cruz	sc-374015	WB
Histone1 H3D	Histone1 H3D	Mouse	Santa Cruz	sc-134355	WB
Cul4	Cul4 (H11)	Mouse	Santa Cruz	sc-377188	WB
Des	Desmin	Rabbit	Abcam	ab15200	WB
eEF2	eEF2	Rabbit	Cell Signaling	2332s	WB
rpS20	rpS20	Rabbit	Abcam	ab133776	WB
Raptor	Raptor	Rabbit	Bethyl Laboratories	A300-553A	WB
TSC2	Tuberin/TSC2 (D93F12)	Rabbit	Cell Signaling	4308T	WB

LUMistar OPTIMA plate reader. Luciferase's signals were normalized to total protein amount determined with RC-DC kit (Bio-Rad).

Statistics

In vivo experiments were performed on 3–15 biological replicates (mice) for each treatment. Throughout the studies, the investigators were blinded to the sample group allocation during the experiment and analysis of the experimental outcome. Statistical analysis was performed using GraphPad Prism 7.0 (GraphPad Software Inc.; www.graphpad.com) or R.

All the data sets were tested for normality of distribution using the Shapiro–Wilks test (threshold $P < 0.05$). For normally distributed data, values shown are mean ± SEM. Statistical analysis of data involving two groups was performed using unpaired two-tailed *t*-test, for more than two groups 1-way ANOVA with the Bonferroni test

applied to correct for multiple comparisons. Sequencing count data were modeled using negative-binomial distribution.

For not normally distributed data, a nonparametric test was used to test for significance between different groups. A Mann–Whitney test was performed when comparing two groups. A Kruskal–Wallis test was used when comparing multiple groups (more than two) followed by Dunn's multiple test comparison.

Data availability

Raw sequencing data have been made publicly available and can be accessed.

RNA-Seq: Raw data have been uploaded to GEO (accession ID: GSE153364; <https://www.ncbi.nlm.nih.gov/gds/?term=GSE153364>).

Ribo-Seq: Raw data have been uploaded to SRA (accession ID: SRP156230; <https://www.ncbi.nlm.nih.gov/sra/?term=SRP156230>).

Expanded View for this article is available online.

Acknowledgments

A.A.G., H.A.K., M.V., S.D., and C.D. acknowledge the DZHK (German Centre for Cardiovascular Research) Partner Site Heidelberg/Mannheim. C.D. acknowledges funding from the Klaus-Tschira Stiftung GmbH. S.D. acknowledges the European Society of Cardiology Basic Research Fellowship and the DZHK Excellence Programme. M.V. acknowledges the DFG (German Research Foundation, DFG VO 1659 2/1, DFG VO 1659 2/2, DFG VO 1659 4/1, DFG VO 1659 6/1), the Boehringer Ingelheim Foundation (Plus 3 Programme). Open Access funding enabled and organized by Projekt DEAL.

Author contributions

SD and MV conceptualized the data; AAG, CS, ER, CH, EM, EV, VK, JÖ, LJ, VK-S, CS, JF curated the data; MHK, CS, EB, and CD made formal analysis; NF, HAK, SD, and MV acquired funding; EB, CD, SD, and MV contributed to methodology; CS, LJ, and VKS contributed to project administration; SD and MV supervised the study; AAG and MV visualized the data; AAG contributed to writing—original draft; NF, HAK, SD, and MV contributed to writing—review and editing.

Conflict of interest

All authors declare that they have no conflict of interest.

References

- Aoki T, Okada N, Ishida M, Yogosawa S, Makino Y, Tamura TA (1999) TIP120B: A novel TIP120-family protein that is expressed specifically in muscle tissues. *Biochem Biophys Res Commun* 261: 911–916
- Avni D, Biberman Y, Meyuhos O (1996) The 5' terminal oligopyrimidine tract confers translational control on top mRNAs in a cell type- and sequence context-dependent manner. *Nucleic Acids Res* 25: 995–1001
- Backman TWH, Girke T (2016) systemPipeR: NGS workflow and report generation environment. *BMC Bioinformatics* 17: 388
- Buss SJ, Muenz S, Riffel JH, Malekar P, Hagenmueller M, Weiss CS, Bea F, Bekeredjian R, Schinke-Braun M, Izumo S et al (2009) Beneficial effects of mammalian target of rapamycin inhibition on left ventricular remodeling after myocardial infarction. *J Am Coll Cardiol* 54: 2435–2446
- Cannavo A, Liccardo D, Eguchi A, Elliott KJ, Traynham CJ, Ibbett J, Eguchi S, Leosco D, Ferrara N, Rengo G et al (2016) Myocardial pathology induced by aldosterone is dependent on non-canonical activities of G protein-coupled receptor kinases. *Nat Commun* 7: 10877
- Doroudgar S, Hofmann C, Boileau E, Malone B, Riechert E, Gorska AA, Jakobi T, Sandmann C, Jürgensen L, Kmietczyk V et al (2019) Monitoring cell-type-specific gene expression using ribosome profiling in vivo during cardiac hemodynamic stress. *Circ Res* 125: 431–448
- Draws O, Taegtmeier H (2014) Targeting the ubiquitin-proteasome system in heart disease: the basis for new therapeutic strategies. *Antioxidants Redox Signal* 21: 2322–2343.
- Ehler E, Moore-Morris T, Lange S (2013) Isolation and culture of neonatal mouse cardiomyocytes. *J Vis Exp* 50154
- Furukawa M, Zhang Y, McCarville J, Ohta T, Xiong Y (2000) The CUL1 C-terminal sequence and ROC1 are required for efficient nuclear accumulation, NEDD8 modification, and ubiquitin ligase activity of CUL1. *Mol Cell Biol* 20: 8185–8197
- Gold JI, Martini JS, Hullmann J, Gao E, Chuprun JK, Lee L, Tilley DG, Rabinowitz JE, Bossuyt J, Bers DM et al (2013) Nuclear translocation of cardiac G protein-coupled receptor kinase 5 downstream of select Gq-activating hypertrophic ligands is a calmodulin-dependent process. *PLoS One* 8: e57324
- Goldenberg SJ, Cascio TC, Shumway SD, Garbutt KC, Liu J, Xiong Y, Zheng N (2004) Structure of the Cand1-Cul1-Roc1 complex reveals regulatory mechanisms for the assembly of the multisubunit cullin-dependent ubiquitin ligases. *Cell* 119: 517–528
- Gregers E, Ahlberg G, Christensen T, Jabbari J, Larsen KO, Herfelt CB, Henningsen KM, Andreasen L, Thiis JJ, Lund J et al (2017) Deep sequencing of atrial fibrillation patients with mitral valve regurgitation shows no evidence of mosaicism but reveals novel rare germline variants. *Heart Rhythm* 14: 1531–1538
- Hsieh AC, Liu YI, Edlind MP, Ingolia NT, Janes MR, Sher A, Shi EY, Stumpf CR, Christensen C, Bonham MJ et al (2012) The translational landscape of mTOR signalling steers cancer initiation and metastasis. *Nature* 485: 55–61
- Huang HT, Brand OM, Mathew M, Ignatiou C, Ewen EP, McCalmon SA, Naya FJ (2006) Myomaxin is a novel transcriptional target of MEF2A that encodes a Xin-related α -actinin-interacting protein. *J Biol Chem* 281: 39370–39379
- Iadevaia V, Zhang Z, Jan E, Proud CG (2012) mTOR signaling regulates the processing of pre-rRNA in human cells. *Nucleic Acids Res* 40: 2527–2539
- Ingolia NT, Ghaemmaghami S, Newman JRS, Weissman JS (2009) Genome-wide analysis in vivo of translation with nucleotide resolution using ribosome profiling. *Science* 324: 218–223
- Jefferies HB, Reinhard C, Kozma SC, Thomas G (1994) Rapamycin selectively represses translation of the 'polypyrimidine tract' mRNA family. *Proc Natl Acad Sci USA* 91: 4441–4445
- Johnson LR, Scott MGH, Pitcher JA (2004) G protein-coupled receptor kinase 5 contains a DNA-binding nuclear localization sequence. *Mol Cell Biol* 24: 10169–10179
- Kim D, Perlea G, Trapnell C, Pimentel H, Kelley R, Salzberg SL (2013) TopHat2: Accurate alignment of transcriptomes in the presence of insertions, deletions and gene fusions. *Genome Biol* 14: R36
- Kmietczyk V, Riechert E, Kalinski L, Boileau E, Malovrh E, Malone B, Gorska A, Hofmann C, Varma E, Jürgensen L et al (2019) mTOR A-mRNA methylation regulates cardiac gene expression and cellular growth. *Life Sci Alliance* 2: e201800233
- Lehmann LH, Jebessa ZH, Kreusser MM, Horsch A, He T, Kronlage M, Dewenter M, Sramek V, Oehl U, Krebs-Haupenthal J et al (2018) A proteolytic fragment of histone deacetylase 4 protects the heart from failure by regulating the hexosamine biosynthetic pathway. *Nat Med* 24: 62–72
- Liu J, Furukawa M, Matsumoto T, Xiong Y (2002) NEDD8 modification of CUL1 dissociates p120CAND1, an inhibitor of CUL1-SKP1 binding and SCF ligases. *Mol Cell* 10: 1511–1518
- Liu X, Reitsma JM, Mamrosh JL, Zhang Y, Straube R, Deshaies RJ (2018) Cand1-mediated adaptive exchange mechanism enables variation in F-box protein expression. *Mol Cell* 69: 773–786
- Ma XM, Blenis J (2009) Molecular mechanisms of mTOR-mediated translational control. *Nat Rev Mol Cell Biol* 10: 307–318
- Malone B, Atanassov I, Aeschmann F, Li X, Großhans H, Dieterich C (2016) Bayesian prediction of RNA translation from ribosome profiling. *Nucleic Acids Res* 45: 2960–2972
- Martini JS, Raake P, Vinge LE, DeGeorge BR, Chuprun JK, Harris DM, Gao E, Eckhart AD, Pitcher JA, Koch WJ (2008) Uncovering G protein-coupled receptor kinase-5 as a histone deacetylase kinase in the nucleus of cardiomyocytes. *Proc Natl Acad Sci USA* 105: 12457–12462

- Min KW, Kwon MJ, Park HS, Park Y, Sungjoo KY, Yoon JB (2005) CAND1 enhances deneddylation of CUL1 by COP9 signalosome. *Biochem Biophys Res Commun* 334: 867–874
- Moriyama H, Yamamoto T, Oiwana H, Tonegawa K, Tsuchiyama D, Kawakatsu I, Obana M, Maeda M, Mohri T, Obika S et al (2017) Phospholamban inhibition by a single dose of locked nucleic acid antisense oligonucleotide improves cardiac contractility in pressure overload-induced systolic dysfunction in mice. *J Cardiovasc Pharmacol Ther* 22: 273–282
- Poulin F, Gingras AC, Olsen H, Chevalier S, Sonenberg N (1998) 4E-BP3, a new member of the eukaryotic initiation factor 4E-binding protein family. *J Biol Chem* 273: 14002–14007
- Robinson MD, McCarthy DJ, Smyth GK (2010) edgeR: a Bioconductor package for differential expression analysis of digital gene expression data. *Bioinformatics* 26: 139–140.
- Sanalip A, Schumacher D, Kiper L, Varma E, Riechert E, Ho TC, Hofmann C, Kmietczyk V, Zimmermann F, Dlugosz S et al (2020) Saraf-dependent activation of mTORC1 regulates cardiac growth. *J Mol Cell Cardiol* 141: 30–42
- Sciarretta S, Forte M, Frati G, Sadoshima J (2018) New insights into the role of mTOR signaling in the cardiovascular system. *Circ Res* 122: 489–505
- Shioi T, McMullen JR, Tarnavski O, Converso K, Sherwood MC, Manning WJ, Izumo S (2003) Rapamycin attenuates load-induced cardiac hypertrophy in mice. *Circulation* 107: 1664–1670
- Shiraishi S, Zhou C, Aoki T, Sato N, Chiba T, Tanaka K, Yoshida S, Nabeshima Y, Nabeshima Y, Tamura T (2007) TBP-interacting Protein 120B (TIP120B)/Cullin-associated and Neddylation-dissociated 2 (CAND2) Inhibits SCF-dependent ubiquitination of myogenin and accelerates myogenic differentiation. *J Biol Chem* 282: 9017–9028
- Sinner MF, Tucker NR, Lunetta KL, Ozaki K, Smith JG, Trompet S, Bis JC, Lin H, Chung MK, Nielsen JB et al (2014) Integrating genetic, transcriptional, and functional analyses to identify 5 novel genes for atrial fibrillation. *Circulation* 130: 1225–1235
- Su H, Li J, Menon S, Liu J, Kumarapeli AR, Wei N, Wang X (2011) Perturbation of cullin deneddylation via conditional Csn8 ablation impairs the ubiquitin-proteasome system and causes cardiomyocyte necrosis and dilated cardiomyopathy in mice. *Circ Res* 108: 40–50
- Su H, Li J, Osinska H, Li F, Robbins J, Liu J, Wei N, Wang X (2013) The COP9 signalosome is required for autophagy, proteasome-mediated proteolysis, and cardiomyocyte survival in adult mice. *Circ Hear Fail* 6: 1049–1057
- Thoreen CC, Chantranupong L, Keys HR, Wang T, Gray NS, Sabatini DM (2012) A unifying model for mTORC1-mediated regulation of mRNA translation. *Nature* 485: 109–113
- Traynham CJ, Hullmann J, Koch WJ (2016) Canonical and non-canonical actions of GRK5 in the heart. *J Mol Cell Cardiol* 92: 196–202
- van Heesch S, Witte F, Schneider-Lunitz V, Schulz JF, Adami E, Faber AB, Kirchner M, Maatz H, Blachut S, Sandmann C-L et al (2019) The translational landscape of the human heart. *Cell* 178: 242–260
- Völkers M, Doroudgar S, Nguyen N, Konstandin MH, Quijada P, Din S, Ornelas L, Thuerauf DJ, Gude N, Friedrich K et al (2014) PRAS40 prevents development of diabetic cardiomyopathy and improves hepatic insulin sensitivity in obesity. *EMBO Mol Med* 6: 57–65
- Volkers M, Toko H, Doroudgar S, Din S, Quijada P, Joyo AY, Ornelas L, Joyo E, Thuerauf DJ, Konstandin MH et al (2013) Pathological hypertrophy amelioration by PRAS40-mediated inhibition of mTORC1. *Proc Natl Acad Sci USA* 110: 12661–12666
- Wei T, Song J, Xu M, Lv L, Liu C, Shen J, Huang Y (2016) NEURL rs6584555 and CAND2 rs4642101 contribute to postoperative atrial fibrillation: a prospective study among Chinese population. *Oncotarget* 7: 42617–42624
- Wysocka J, Reilly PT, Herr W (2001) Loss of HCF-1—Chromatin association precedes temperature-induced growth arrest of tsBN67 cells. *Mol Cell Biol* 21: 3820–3829
- Zhang D, Contu R, Latronico MVG, Zhang JL, Rizzi R, Catalucci D, Miyamoto S, Huang K, Ceci M, Gu Y et al (2010) mTORC1 regulates cardiac function and myocyte survival through 4E-BP1 inhibition in mice. *J Clin Invest* 120: 2805–2816
- Zhang Y, Matkovich SJ, Duan X, Gold JJ, Koch WJ, Dorn GW (2011) Nuclear effects of G-protein receptor kinase 5 on histone deacetylase 5-regulated gene transcription in heart failure. *Circ Hear Fail* 4: 659–668
- Zheng N, Schulman BA, Song L, Miller JJ, Jeffrey PD, Wang P, Chu C, Koepf DM, Elledge SJ, Pagano M et al (2002) Structure of the Cul1–Rbx1–Skp1–F-box Skp2 SCF ubiquitin ligase complex. *Nature* 416: 703–709
- Zou J, Ma W, Li J, Littlejohn R, Zhou H, Kim I-M, Fulton DJR, Chen W, Weintraub NL, Zhou J et al (2018) Neddylation mediates ventricular chamber maturation through repression of Hippo signaling. *Proc Natl Acad Sci USA* 115: E4101–E4110
- Zou J, Ma W, Littlejohn R, Li J, Stansfield BK, Kim IM, Liu J, Zhou J, Weintraub NL, Su H (2019) Transient inhibition of neddylation at neonatal stage evokes reversible cardiomyopathy and predisposes the heart to isoproterenol-induced heart failure. *Am J Physiol - Hear Circ Physiol* 316: H1406–H1416



License: This is an open access article under the terms of the Creative Commons Attribution-NonCommercial-NoDerivs License, which permits use and distribution in any medium, provided the original work is properly cited, the use is non-commercial and no modifications or adaptations are made.